

ATLAS CONF Note

ATLAS-CONF-2025-006

7th July 2025



Combined measurements of Higgs boson production and decay at $\sqrt{s} = 13$ TeV using up to 140 fb⁻¹ of data collected by the ATLAS Experiment

The ATLAS Collaboration

This note presents combined measurements of Higgs boson production and decay using up to 140 fb⁻¹ of proton-proton collision data collected by the ATLAS experiment at the LHC at $\sqrt{s} = 13$ TeV. The global signal strength is determined to be $1.023^{+0.056}_{-0.053}$. Measurements of inclusive production cross-sections, decay branching ratios, production cross-sections for individual decay channels, and Higgs boson coupling modifiers are also presented and discussed. The cross-sections for Higgs boson production in association with W bosons, Z bosons, or top quarks is measured with a precision that is improved by 20-40% relative to the most recent comparable results from the ATLAS Collaboration. Uncertainties in the measurements of Higgs boson branching ratios to WW, bb, and $\tau\tau$ are similarly reduced by 10-20%. Higgs boson couplings to W, Z, t, b, and τ are determined with an accuracy that is improved by 10-20%, and about 50% for the coupling to the charm quark.

Contents

1	Introduction	2
2	ATLAS detector	3
3	Input measurements and combination procedure	4
4	Results 4.1 Measurement of the global signal strength	6
	4.2 Cross-section measurements in production modes	7
	4.3 Decay branching ratio measurements	8
	4.4 Production and decay measurements	10
	4.5 Measurements of couplings parameters in the κ framework	12
5	Conclusion	17
Aj	ppendix	18
A	Coupling modifier parameterization	18
В	Expected signal strength results	18
C	Additional production cross-section and branching ratio results	20
D	25	
E	Additional results including partial Run 3 data	29

1 Introduction

One of the main physics objectives of Run 2 of the LHC (2015-2018) has been to measure with increasing precision the properties of the Higgs boson discovered by the ATLAS and CMS Collaborations in 2012 [1, 2]. These properties were so far found to be compatible with those predicted for the Higgs boson in the Standard Model (SM) of particle physics. Precise measurements of these properties therefore provide a test of the consistency of the SM and a window into possible new phenomena beyond it.

Within the SM, the couplings of the Higgs boson to fundamental SM particles and the rates of its production and decay processes are fully determined from the knowledge of SM parameters. ATLAS and CMS have performed measurements of these properties using analyses targeting a variety of Higgs boson production and decay channels. The production processes considered consist of gluon–gluon fusion (ggF), weak vector-boson fusion (VBF), associated production with a weak vector boson (VH, with V=W,Z), and associated production with a pair of top quarks, (ttH), a pair of b-quarks (bbH) or a single top quark

(tH). The decay channels include $H \to bb$, $H \to WW^* \to \ell \nu \ell \nu$, $H \to \tau \tau$, $H \to cc$, $H \to ZZ^* \to 4\ell$, $H \to \gamma \gamma$, $H \to Z\gamma$, and $H \to \mu \mu$. These processes are illustrated in Figure 1.

This note studies the production and decay rates of the Higgs boson, using a combination of analyses targeting individual production and decay processes. Compared to the previously published combination of Ref. [3], six new or updated measurements are included, with significant improvements to the measurements of the $H \to \tau\tau$, $H \to WW^*$, $VH(\to bb, cc)$, and $ttH(\to bb)$ processes.

All analyses use the full dataset of pp collisions collected during Run 2, except for that of Ref. [4] which uses only data collected in 2015 and 2016 and that of Ref. [5] which uses triggers that were not available during part of Run 2. The results assume the value $m_H = 125.09 \pm 0.24$ GeV for the Higgs boson mass, as obtained from the latest combination of ATLAS and CMS measurements [6], and compatible with more recent measurements performed individually by ATLAS [7, 8] and CMS [9, 10].

Results are reported in terms of the inclusive rates of the production and decay processes mentioned above, and interpreted as modifications to the Higgs boson couplings within the κ framework [11].

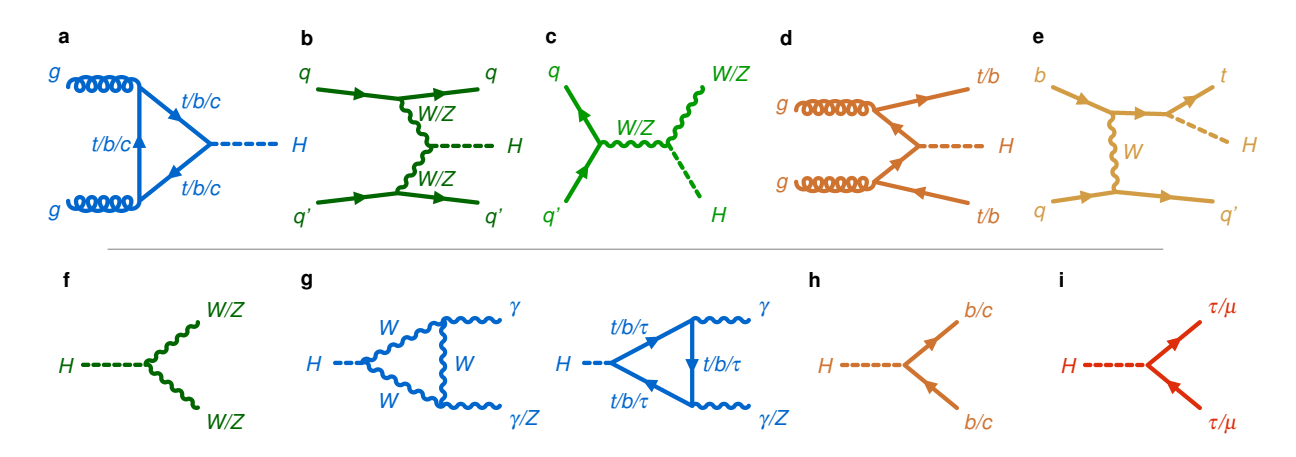


Figure 1: Examples of Feynman diagrams for Higgs boson production (top row) and decay (bottom row): Higgs boson production via gluon–gluon fusion (ggF; a), weak vector-boson fusion (VBF; b), and associated production with vector bosons (VH; c), top- or b-quark pairs (ttH, bbH; d), or a single top quark (tH; e); Higgs boson decays into a pair of vector bosons (f), a pair of photons or a f boson and a photon (f), a pair of quarks (f), and a pair of charged leptons (f). Loop-induced Higgs boson interactions with gluons or photons are shown in blue, processes involving couplings to f0 or f1 bosons in green, to quarks in orange, and to leptons in red. Two different shades of green (orange) are used to separate the VBF and f1 and f2 production processes.

2 ATLAS detector

The ATLAS experiment [12] at the LHC is a multipurpose particle detector with a forward–backward symmetric, cylindrical geometry and a near 4π coverage in solid angle. The detector records digitized signals produced by the products of LHC's proton bunch collisions, hereafter termed collision 'events'. It is designed to identify a wide variety of particles and measure their momenta and energies. These particles include electrons, muons and τ -leptons, photons, as well as gluons and quarks which produce collimated

¹ No distinction is made between particles and antiparticles, and the same notation is used to refer to both. ℓ refers to electrons and muons.

jets of particles in the detector. Since the jets from b-quarks and c-quarks contain hadrons with relatively long lifetimes, they can be identified by observing a decay vertex which typically occurs at a measurable distance from the collision point. The presence of particles that do not interact with the detector, such as neutrinos, can be inferred by summing the vector momenta of the visible particles in the plane transverse to the beam and imposing conservation of transverse momenta.

The detector components closest to the collision point measure charged-particle trajectories and momenta. This inner spectrometer is surrounded by calorimeters that are used in the identification of particles and in the measurement of their energies. The calorimeters are in turn surrounded by an outer spectrometer dedicated to measuring the trajectories and momenta of muons, the only charged particle to travel through the calorimeters. A two-level trigger system was optimized for Run 2 data-taking [13] to select events of interest at a rate of about 1 kHz from the proton bunch collisions occurring at a rate of 40 MHz. An extensive software suite [14] is used in the simulation, reconstruction and analysis of real and simulated data, in detector operations, and in the trigger and data acquisition systems of the experiment.

3 Input measurements and combination procedure

Analyses of Higgs boson processes typically measure Higgs boson event rates in specific production and decay processes. This measurement is performed either inclusively, or differentially in the kinematics of the production process within the Simplified Template Cross-section (STXS) framework [15–17]. To this end the analysis also accounts for background processes, which are suppressed using several methods. To obtain the most accurate measurement of the Higgs boson interactions a simultaneous fit is performed on a combined set of complementary measurements, under a number of physically motivated assumptions. The relative contribution of each process in the combined fit depends on the expected signal rates for the studied Higgs processes, the selection efficiency of the analysis, the signal-to-background ratios, and the associated systematic uncertainties.

The single-process measurements entering the combination are listed in Table 1, including references to the results of the single-process measurements. In some cases these input analyses have been modified compared to their publication: in particular, analysis results using the value of 139 fb⁻¹ for the integrated luminosity of the Run 2 dataset have been modified to reflect the updated value of 140 fb⁻¹ and its associated relative uncertainty of 0.83% [18].

The SM is tested by comparing the observed signal rates to theory predictions that use the most recent calculations of Higgs boson production cross sections and branching ratios (see Refs. [16, 29–34]). These predictions assume the common value $m_H = 125.09 \pm 0.24$ GeV; the single-process measurements have been adjusted to use this reference when necessary.

All signal trigger and reconstruction efficiencies and most background rates are predicted from the simulation. The simulation is complemented by the use of dedicated, signal-depleted control data for measurements of selected background processes and to constrain selection efficiencies. A common set of event generators are used in all analyses to describe the physics processes in the proton–proton collisions. The generated events are passed through a detailed simulation of the ATLAS detector and trigger response prior to their reconstruction and identification.

The measurement parameters, also referred to as parameters of interest (POIs), represent signal rates in the various analysis regions in terms of Higgs boson production cross sections, decay branching ratios, or coupling modifiers within the κ framework. Different parameterisations are used to interpret the data under different physics assumptions.

Table 1: Input analyses to the combination with their integrated luminosity (\mathcal{L}), reference to the original publication and STXS granularity. Analyses initially reporting results corresponding to a Run 2 integrated luminosity of 139 fb⁻¹ are rescaled to the updated 140 fb⁻¹ value for the combination. In the last column, *New analysis* denotes analyses not present in the combination reported in Ref. [3]; *Full Run* 2 refers to analyses that used a partial Run 2 dataset and have been updated to the full dataset; and *Reanalysis* to cases where an improved analysis of the full Run 2 dataset is used.

Analysis	Prod.	£	Reference	STXS	Improvements
	modes	(fb^{-1})		stage	relative to Ref. [3]
$H \to ZZ^* \to 4\ell$	All	140	[19]	1.2	-
$H \to WW^* \to \ell \nu \ell \nu$	ggF,VBF	140	[20]	0	Reanalysis
$H \to WW^* \to \ell \nu \ell \nu$	VH	140	[21]	1.2	Full Run 2
$H o \gamma \gamma$	All	140	[22]	1.2	-
$H \rightarrow Z \gamma$	All	140	[23]	0	-
H o au au	All	140	[24]	1.2	Reanalysis
H o au au	VH	140	[25]	0	New analysis
$H \rightarrow \mu\mu$	All	140	[26]	0	-
$H \rightarrow bb$	VBF	126	[5]	1.2	-
$H \rightarrow bb, cc$	VH	140	[27]	1.2	Reanalysis
$H \rightarrow \text{multileptons}$	ttH	36.1	[4]	0	-
$H \rightarrow bb$	ttH	140	[28]	1.2	Reanalysis

The statistical analysis of the data relies on a likelihood formalism, where the product of the likelihood functions describing each of the input measurements is calculated in order to obtain a combined likelihood [35]. The effects of experimental and theoretical systematic uncertainties on the predicted signal and background yields are taken into account by including nuisance parameters (NPs) in the likelihood function, which are free to vary in the fit. Some of these parameters, referred to as *unconstrained*, are determined from data only. Other parameters, referred to as *constrained*, are also subject to a constraint by an *auxiliary* measurement and quantify the effect of systematic uncertainties. Auxiliary measurements are usually represented by a unit-Gaussian constraint with a mean corresponding to the NP, or in some cases by a Poisson distribution. In most cases, the impact of Gaussian-contrained NPs on other parameters in the likelihood is implemented using an exponential form, which is equivalent to the use of a log-normal constraint. The observable of the constraint distribution is the *global observable* representing the observed value of the auxiliary measurement [35]. When the same systematic uncertainty source affects multiple analysis channels, a correlated uncertainty is implemented by using the same NP in each case.

The statistical test of a given signal hypothesis, used for the measurement of the parameters of interest, is performed with a test statistic based on the profile likelihood ratio [36]. The confidence intervals of the measured parameters are obtained using asymptotic formulae [36]. The compatibility of the results and the SM predictions is estimated using a p-value p_{SM} computed as described in Ref. [3].

The combined likelihood is obtained by including all the categories c from each input analysis a, and the constraints for all constrained nuisance parameters. It can be written as

$$\mathcal{L}(\boldsymbol{\mu}, \boldsymbol{\theta}; \text{data}) = \prod_{a=1}^{N_{\text{inputs}}} \prod_{c=1}^{N_{\text{cats}}} \mathcal{L}_{c}^{(a)}(\boldsymbol{\mu}, \boldsymbol{\theta}; \text{data}) \prod_{k=1}^{N_{\text{cons}}} \mathcal{G}\left(\tilde{\theta}_{k}; \theta_{k}\right), \tag{1}$$

where μ and θ are the vectors of POIs and NPs respectively, $N_{\rm inputs}$ is the number of input analyses a, $N_{\rm cats}^{(a)}$ is the number of categories in analysis a, $\mathcal{L}_c^{(a)}$ is the likelihood function for category c of analysis a, $N_{\rm cons}$ is the overall number of constrained nuisance parameters, \mathcal{G} denotes the constraint PDF and $\tilde{\theta}_k$ is the global observable corresponding to θ_k . The signal-sensitive regions of all input analyses are non-overlapping by construction. In some cases, the selections of the control regions used to constrain background processes have a small overlap with regions in other analyses. The effect of these overlaps is however found to be very small compared to uncertainties of the results and their effect is not considered in the statistical treatment.

Uncertainties on the Higgs boson production cross-sections are applied on the predicted cross-sections in each region of the STXS Stage 1.2 scheme, as described in Ref. [3], and uncertainties on Higgs boson branching ratios are applied as prescribed in Ref. [16]. These theory uncertainties, along with experimental systematic uncertainties and uncertainties on the luminosity measurement, are considered to be correlated across analyses, and implemented in the likelihood using the prescription described above. Other sources of theory uncertainty are implemented as uncorrelated. Some NPs initially implemented as correlated are decorrelated if the corresponding NPs are found to have large best-fit values or reduced uncertainties in fits to data in each input channel.

Uncertainties are decomposed into components corresponding to different classes of uncertainty following a method similar to the one used in Ref. [3]. The NPs corresponding to a given class of uncertainty are fixed to their best-fit value, and the uncertainty component is obtained by subtracting in quadrature the uncertainty obtained in a fit performed in this configuration from the uncertainty obtained in the original fit. The statistical uncertainty component is obtained in a fit where all NPs are fixed to their best-fit values.

4 Results

4.1 Measurement of the global signal strength

The rate of Higgs boson production and decay processes is expressed using the quantity $\sigma_i \times B_f$, where σ_i denotes the cross-section of the production process i and B_f the branching ratio into the final state f. The signal strength of the process is defined by the ratio $\mu_{if} = (\sigma_i \times B_f)/(\sigma_i^{\text{SM}} \times B_f^{\text{SM}})$ of the measured event rate to its SM prediction.

This section presents the measurement of a single signal strength μ scaling all event rates considered in the combination. The measurement yields

$$\mu = 1.023^{+0.056}_{-0.053} = 1.023 \pm 0.028 \text{ (stat.)} ^{+0.026}_{-0.025} \text{ (exp.)} ^{+0.039}_{-0.036} \text{ (sig. theo.)} \pm 0.012 \text{ (bkg. theo.)}$$

where (stat.) refers to the statistical component of the uncertainty, (exp.) to the contribution from experimental systematic uncertainty, (sig. theo.) to theory uncertainties on the Higgs boson signal, and (bkg. theo.) to theory uncertainties on the background processes. It can be noted that the overall theory uncertainty is larger than both the experimental systematic uncertainty and the statistical uncertainty. The expected result under SM assumptions is $1.000^{+0.055}_{-0.053}$. The observed profile log-likelihood scan is shown in Figure 2.

The result is in good agreement with the SM, with a compatibility corresponding to a p-value $p_{SM} = 68\%$. The total uncertainty is reduced by about 10% compared to the results published in Ref. [3].

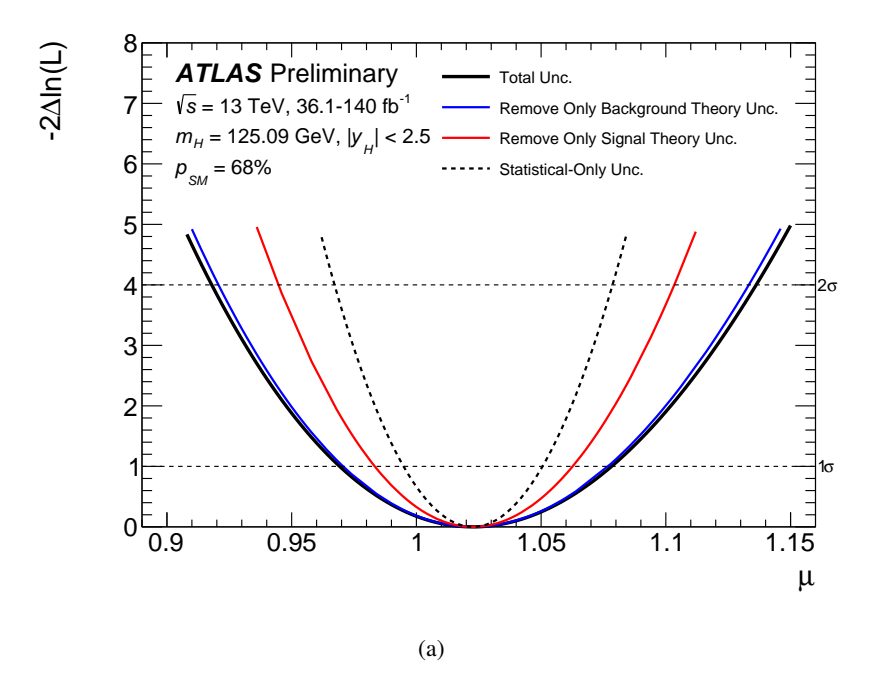


Figure 2: Observed profile log-likelihood value as a function of the signal strength μ , in the model with a single signal-strength scaling all processes. The intersections with the horizontal dotted lines define the 1σ and 2σ uncertainties on the measurement. The solid black line corresponds to the full statistical model with all uncertainties included, and other lines to cases where a class of systematic uncertainties is removed from consideration as described in the text: the background theory uncertainties (blue line), the signal theory uncertainties (red line), and all systematic uncertainties (dashed black line).

4.2 Cross-section measurements in production modes

A measurement of the production cross-sections of Higgs boson production processes is performed assuming that the branching ratios of Higgs boson decays are equal to their SM expectations, within SM theory uncertainties. The bbH mode is considered together with ggF since no dedicated analysis targeting this process is included in the combination and the acceptances for the bbH and ggF processes are similar in all the channels considered. Similarly, the tH process is considered together with ttH. The other production modes considered are VBF, WH and ZH. The VH process includes both leptonic and hadronic decays of the W and Z, and the $gg \rightarrow ZH$ process is considered as part of ZH. Cross-sections are reported in the fiducial volume $|y_H| < 2.5$, where y_H is the rapidity of the Higgs boson, which matches to a good approximation the detector region over which the Higgs boson decay products can be reconstructed across the analyses in the combination.

The observed results are shown in Figure 3 and Table 2. The results are in agreement with SM predictions, with a p-value $p_{\text{SM}} = 97\%$.

Compared to the previous combination of Ref. [3], uncertainties on σ_{WH} and σ_{ZH} are reduced by about 30% and 20%, respectively, mainly as a result of the updated measurement of $VH(\rightarrow bb, cc)$ [27]. Similarly, the uncertainty on σ_{ttH} is reduced by about 40%, mainly due to the updated measurement of $ttH(\rightarrow bb)$ [28].

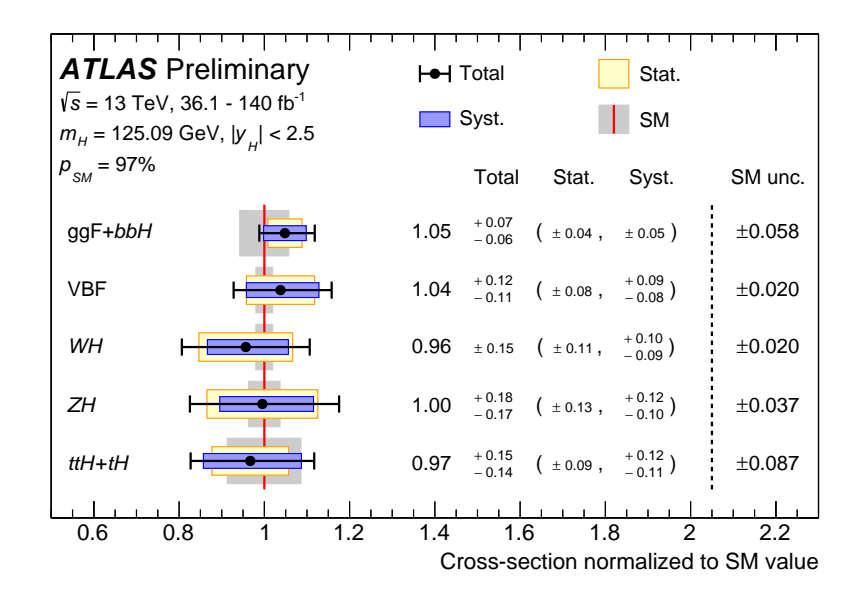


Figure 3: Observed cross-sections values for the main Higgs boson production modes, relative to their SM predictions. The bbH mode is considered together with ggF, and tH with ttH. Higgs boson decay branching ratios are assumed to be equal to their SM predictions.

Table 2: Measured values of Higgs boson production cross-sections, assuming branching ratios to match their expectations in the SM. The second column provides the corresponding SM predictions together with the theory uncertainties, and the third column the measured values normalized to the SM predictions.

Cross-section	Measurement (pb)	SM prediction (pb)	Ratio to SM
ggF + bbH	47.0 +3.1 -2.7	44.8 ± 2.6	1.05 +0.07 -0.06
VBF	3.6 ± 0.4	3.50 ± 0.07	$1.04^{+0.12}_{-0.11}$
WH	1.17 ± 0.18	1.216 ± 0.024	0.96 ± 0.15
ZH	0.80 ± 0.14	0.796 ± 0.029	$1.00^{+0.18}_{-0.17}$
ttH + tH	$0.57_{-0.08}^{+0.09}$	0.58 ± 0.05	$0.97^{\ +0.15}_{\ -0.14}$

4.3 Decay branching ratio measurements

A measurement of Higgs boson branching ratios is performed under the assumption that the production cross-sections are equal to their SM expectations, within SM theory uncertainties. Higgs boson processes are considered in the fiducial volume $|y_H| < 2.5$. Observed results are shown in Figure 4 and Table 3. The results are compatible with SM predictions, with a p-value $p_{\rm SM} = 68\%$. Compared to Ref. [3], the uncertainty on the $H \to bb$ branching ratio is reduced by approximately 20%, mainly due to the higher sensitivity of the updated analyses of the $VH(\to bb, cc)$ and $ttH(\to bb)$ processes [27, 28]. The uncertainties on the $H \to WW^*$ and $H \to \tau\tau$ branching ratios are reduced by respectively about 20% and 10% due to the updated analyses of Refs. [20] and [24], as well as to a somewhat lesser degree the analyses

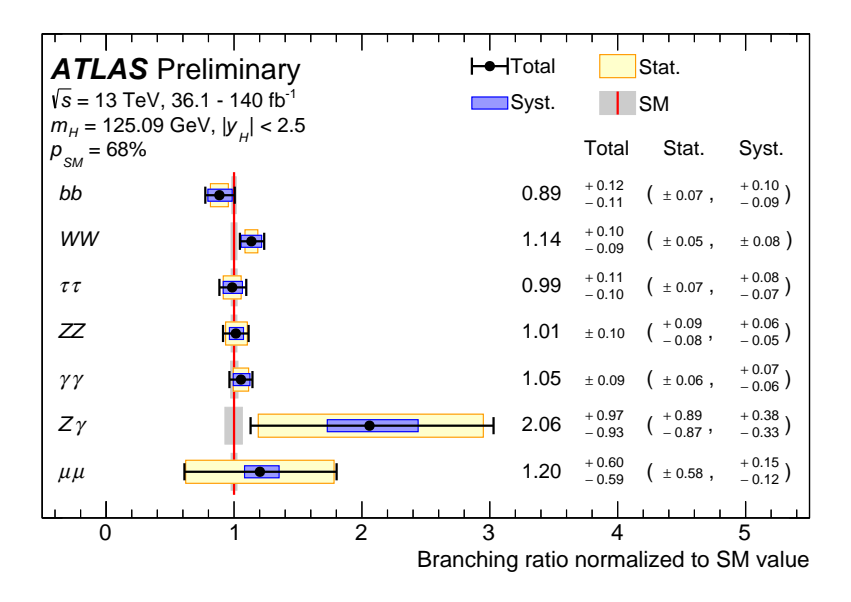


Figure 4: Observed branching ratio values in the $H \to bb$, $H \to WW^*$, $H \to \tau\tau$, $H \to ZZ^*$, $H \to \gamma\gamma$, $H \to Z\gamma$ and $H \to \mu\mu$ decay modes, relative to their SM predictions. Higgs boson production cross-sections are assumed to be equal to their SM predictions.

Table 3: Observed and expected values of Higgs boson decay branching ratios, assuming production cross-sections to match their expectations in the SM. The second column provides the corresponding SM predictions together with the theory uncertainties, and the third column the measured values normalized to the SM predictions.

Branching ratio	Measurement	SM prediction	Ratio to SM
$H \rightarrow bb$	$0.52^{+0.07}_{-0.06}$	0.581 ± 0.010	$0.89^{\ +0.12}_{\ -0.11}$
$H \to WW^*$	$0.245^{+0.022}_{-0.019}$	0.215 ± 0.005	$1.14^{+0.10}_{-0.09}$
$H \to \tau \tau$	$(6.2^{+0.7}_{-0.6}) \cdot 10^{-2}$	$(6.26^{+0.15}_{-0.14}) \cdot 10^{-2}$	$0.99^{+0.11}_{-0.10}$
$H \rightarrow ZZ^*$	$(2.67 \pm 0.26) \cdot 10^{-2}$	$(2.64 \pm 0.06) \cdot 10^{-2}$	1.01 ± 0.10
$H o \gamma \gamma$	$(2.38 \pm 0.20) \cdot 10^{-3}$	$(2.27^{+0.07}_{-0.06}) \cdot 10^{-3}$	1.05 ± 0.09
$H \to Z \gamma$	$(3.2^{+1.5}_{-1.4})\cdot 10^{-3}$	$(1.54^{+0.10}_{-0.11}) \cdot 10^{-3}$	$2.1_{-0.9}^{+1.0}$
$H \to \mu\mu$	$(2.6 \pm 1.3) \cdot 10^{-4}$	$(2.17 \pm 0.05) \cdot 10^{-4}$	1.2 ± 0.6

of Refs. [21] and [25].

4.4 Production and decay measurements

This section presents measurements of Higgs boson production rates for individual decay channels. The $H \to bb$, $H \to WW^*$, $H \to \tau\tau$, $H \to cc$, $H \to ZZ^*$, $H \to \gamma\gamma$, $H \to Z\gamma$, and $H \to \mu\mu$ channels are considered. For production modes, the same scheme is used as in Section 4.2 with some adjustments due to the different sensitivities in some combinations of production and decay final states: in the $H \to bb$ mode, the ggF + bbH and VBF modes are considered as a single process; in the $H \to \gamma\gamma$ mode, the ttH and ttH modes are considered separately; in the $H \to \mu\mu$ decay, the ggF + bbH and ttH + tH modes are similarly considered together, as well as the VBF, WH and ZH modes; in the $H \to Z\gamma$ mode, all production modes are grouped together; and finally in the $H \to cc$ mode, only the WH and ZH processes are considered, while the others are fixed to their SM expectation. In total, 29 combinations ($\sigma_i \times B_f$) of production cross-sections σ_i and branching ratios B_f are reported. Higgs boson signal processes are considered within the fiducial volume $|y_H| < 2.5$.

Results are shown in Figure 5 and Table 4. The results are all in agreement with SM predictions, with a p-value $p_{SM} = 84\%$.

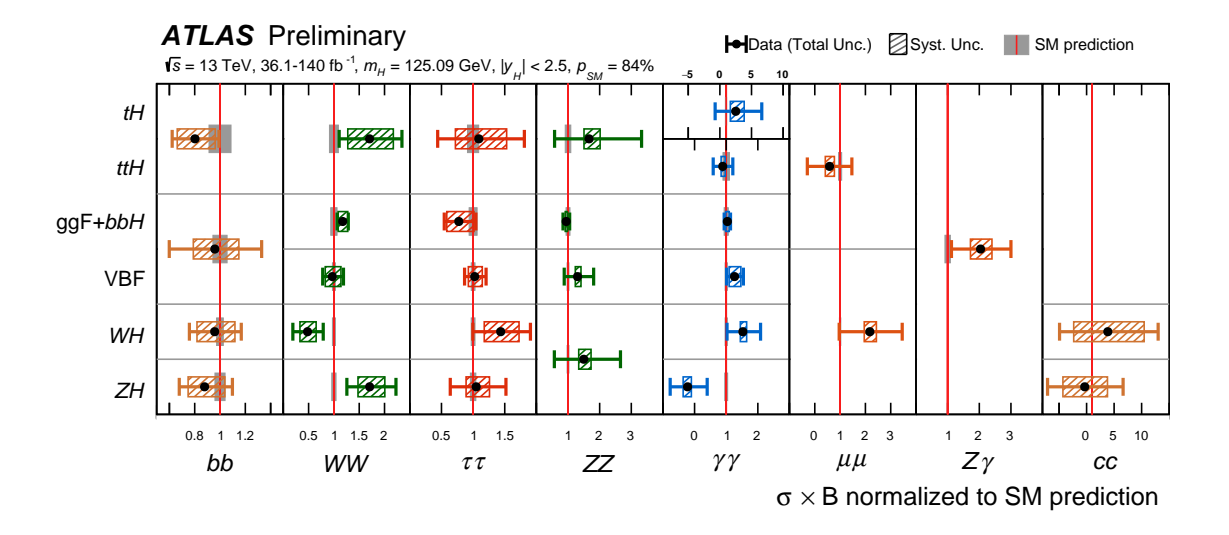


Figure 5: Measured values of $(\sigma_i \times B_f)$ for the combinations of production cross-sections and branching ratios described in the text, relative to their SM predictions.

Table 4: Measured values of $(\sigma_i \times B_f)$ for different combinations of production processes and decay modes. The fourth colum lists the SM prediction for the measuremement together with its theory uncertainty. The values for the $ZH(\to \gamma\gamma)$ and $ZH(\to cc)$ processes are found to be negative due to an observed event count in the corresponding signal-sensitive regions that is below the predicted background level.

Decay mode	Prod. mode	Measurement (pb)	SM prediction (pb)	Ratio to SM
	ggF + bbH + VBF	27 ± 10	28.0 ± 1.6	1.0 ± 0.4
77 . 11	WH	$0.68^{+0.15}_{-0.14}$	$0.706^{+0.018}_{-0.019}$	$0.96^{+0.21}_{-0.20}$
$H \to bb$	ZH	$0.41^{+0.10}_{-0.09}$	0.462 ± 0.019	$0.88^{+0.22}_{-0.20}$
	ttH + tH	0.27 ± 0.06	0.340 ± 0.030	$0.80^{+0.19}_{-0.18}$
	ggF + bbH	11.3 ± 1.1	9.6 ± 0.6	1.17 ± 0.11
	VBF	$0.73^{\ +0.17}_{\ -0.14}$	0.753 ± 0.022	$0.97^{\ +0.22}_{\ -0.19}$
$H \to WW^*$	WH	0.13 ± 0.08	0.262 ± 0.008	$0.48^{\ +0.31}_{\ -0.29}$
	ZH	$0.29 {}^{+0.09}_{-0.08}$	0.171 ± 0.007	$1.7^{+0.5}_{-0.4}$
	ttH + tH	0.21 ± 0.08	0.126 ± 0.011	1.7 ± 0.6
	ggF + bbH	$2.2^{+0.8}_{-0.6}$	2.80 ± 0.17	$0.77^{\ +0.27}_{\ -0.23}$
	VBF	$0.226^{+0.040}_{-0.035}$	0.219 ± 0.007	$1.03^{\ +0.18}_{\ -0.16}$
H o au au	WH	$0.110^{+0.040}_{-0.033}$	0.0761 ± 0.0023	$1.4^{+0.5}_{-0.4}$
	ZH	$0.052 {}^{+0.023}_{-0.020}$	0.0498 ± 0.0022	$1.1^{+0.5}_{-0.4}$
	ttH + tH	$0.040^{+0.026}_{-0.024}$	0.0366 ± 0.0033	1.1 +0.7 -0.6
Decay mode	Prod. mode	Measurement (fb)	SM prediction (fb)	Ratio to SM
$H \rightarrow cc$	WH	$135 ^{+320}_{-310}$	35.1 +2.4 -1.2	3.9 +9.2 -8.8
<i>H</i> → <i>tt</i>	ZH	$-8 ^{+160}_{-150}$	$23.0^{+1.7}_{-1.1}$	$-0.3^{+7.0}_{-6.8}$
	ggF + bbH	$1.11_{-0.12}^{+0.13}$	1.18 ± 0.07	$0.94^{\ +0.11}_{\ -0.10}$
$H \rightarrow ZZ^*$	VBF	$0.12^{\ +0.05}_{\ -0.04}$	0.0924 ± 0.0027	$1.3^{+0.5}_{-0.4}$
11 , 22	VH	$0.08^{\ +0.06}_{\ -0.05}$	$0.0531 {}^{+0.0016}_{-0.0017}$	$1.5^{+1.2}_{-0.9}$
	ttH + tH	$0.026^{+0.026}_{-0.017}$	0.0154 ± 0.0014	1.7 +1.7 -1.1
	ggF + bbH	106 ± 10	102 ± 7	1.04 ± 0.10
	VBF	$10.0^{+2.2}_{-2.0}$	7.94 ± 0.28	$1.26^{+0.28}_{-0.25}$
$H \rightarrow \gamma \gamma$	WH	$4.2^{+1.5}_{-1.4}$	2.76 ± 0.10	$1.5^{+0.6}_{-0.5}$
	ZH	$-0.4^{+1.1}_{-1.0}$	1.81 ± 0.08	-0.2 ± 0.6
	ttH	$1.01 {}^{+0.40}_{-0.34}$	1.13 ± 0.12	$0.89^{+0.32}_{-0.30}$
	tH	$0.5^{+0.8}_{-0.6}$	$0.192 {}^{+0.013}_{-0.025}$	$2.5^{+4.0}_{-3.3}$
$H \to Z\gamma$	All	160 +80 -70	78 ± 7	2.0 +1.0 -0.9
<u> </u>	ggF + bbH + ttH + tH	6 ± 9	9.8 ± 0.6	0.6 ± 0.9
$H \to \mu\mu$	VBF + VH	$2.6_{-1.4}^{+1.5}$	$1.197 {}^{+0.035}_{-0.040}$	$2.2^{+1.3}_{-1.2}$

4.5 Measurements of couplings parameters in the κ framework

The measurements presented in Section 4.4 are interpreted in the context of Higgs boson coupling parameters, which are defined within the κ -framework. Multiplicative modifiers κ_p are introduced for the couplings of the Higgs boson to the elementary SM particles $p = W, Z, t, b, c, \tau, \mu$, with the SM hypothesis corresponding to a unit value for all κ_p . The modifiers κ_g , κ_γ and $\kappa_{Z\gamma}$ are also introduced to describe effective Higgs boson interactions with gluons (Hgg), photons $(H\gamma\gamma)$ and the combined interaction with a photon and a Z boson $(HZ\gamma)$. The rates of Higgs boson processes not probed by the analyses included in the combination are assumed to correspond to their SM expectations, and only SM decays of the Higgs boson are considered. The Higgs boson production cross-sections and decays rates are expressed in terms of the coupling modifiers using several parameterizations, each based on a set of physics assumptions. In each case, the modifications are applied to the SM predictions; the uncertainties in these predictions therefore enter the uncertainties in the measured values of the modifiers.

A first model considers only two coupling modifiers: the bosonic coupling parameters κ_W and κ_Z are assumed to be equal to a single modifier κ_V , while a modifier κ_F is associated to all fermion couplings. Both parameters are assumed to be positive: for κ_V this is by convention, and a negative value of the relative sign between κ_F and κ_V has been experimentally excluded [37]. The effective couplings κ_g , κ_γ and $\kappa_{Z\gamma}$ are expressed as a function of κ_F and κ_V , using expressions derived from the corresponding leading-order loop processes in the SM. The parameterizations used for this model and the ones shown below are described in detail in Table 6 shown in Appendix A.

The observed (expected) values of the coupling modifiers are $\kappa_V = 1.015^{+0.028}_{-0.027}$ (1.000 $^{+0.029}_{-0.026}$) and $\kappa_F = 0.979^{+0.044}_{-0.045}$ (1.000 $^{+0.049}_{-0.043}$). The observed (expected) correlation coefficient between the two parameters is 40% (36%). Profiled log-likelihood contours at 68% and 95% confidence level (CL) in the (κ_V , κ_F) plane are shown in Figure 6. Observed results are consistent with the SM, with a p-value $p_{\rm SM} = 62\%$.

A more general model introduces independent κ modifiers for Higgs boson couplings to each of W, Z, t, b, c, τ and μ . A positive sign is assumed by convention for κ_W . For κ_Z and κ_t only positive values are considered, since the negative regions have been experimentally excluded [37–39]. For κ_b , κ_τ and κ_μ the combination is sensitive to the absolute values of the modifiers but has almost no sensitivity to their signs. Confidence intervals are therefore reported only in the positive region for simplicity. Finally, κ_c is allowed to range over both positive and negative values since it is only weakly constrained and the $\kappa_c = 0$ scenario cannot be excluded at the considered confidence levels.

Two scenarios are explored for the effective modifiers κ_g , κ_γ and $\kappa_{Z\gamma}$: a *resolved* parameterization similar to the first model above, in which the effective modifiers are expressed as functions of the other modifiers using expressions derived from the corresponding leading-order loop contributions within the SM; and an *effective* parameterization in which they are instead considered as independent parameters in the fit. In the resolved parameterization, κ_c is either included as a measurement parameter, or set equal to κ_t .

Coupling modifiers in the resolved parameterization are shown as a function of particle masses in Figure 7, and the measured values for both parameterizations are summarized in Figure 8 and Table 5. The results are consistent with SM expectations, with $p_{SM} = 90\%$ and 82% for the resolved parameterization with and without κ_c as a free parameter, respectively; and $p_{SM} = 89\%$ for the effective parameterization. The uncertainty on the charm coupling modifier κ_c is reduced by a factor of about 2 compared to the results of Ref. [3], mainly due to the improved constraints on the $VH(\to cc)$ process from the analysis of Ref. [27]. The uncertainty on κ_t is improved by about 15% relative to Ref. [3].

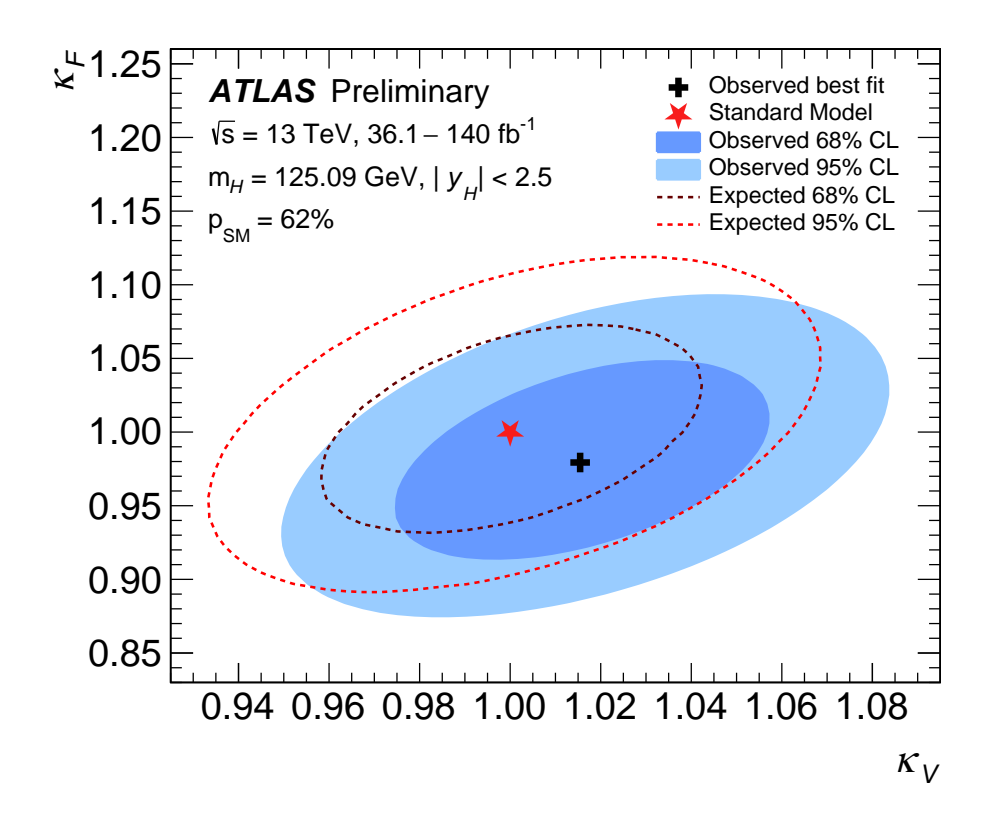


Figure 6: Contours of $-2 \log \Delta L$ in the plane (κ_V, κ_F) of modifiers to Higgs boson fermionic and bosonic coupling modifiers. The observed 68% and 95% CL regions are shown respectively as dark and light blue shaded areas, while the corresponding expected regions under the SM hypothesis are shown in dashed black and red lines, respectively. The black cross indicates the best-fit point, while the SM expectation is represented by the red star.

One can note that the observed values of κ_W and κ_Z in the general model are below 1, whereas in the (κ_V, κ_F) model the value of the common κ_V modifier was above 1. This is related to the fact that in the general model κ_b takes values about one standard deviation below 1, which leads to a value of the total width of the Higgs boson that is below its SM expectation and in turn to smaller values of the other coupling modifiers such as κ_W and κ_Z . In the (κ_V, κ_F) model, κ_b is represented by κ_F , which takes a value closer to 1 due to the effect of other fermionic couplings, and this leads to a higher value of the total width and a thus a higher value of κ_V .

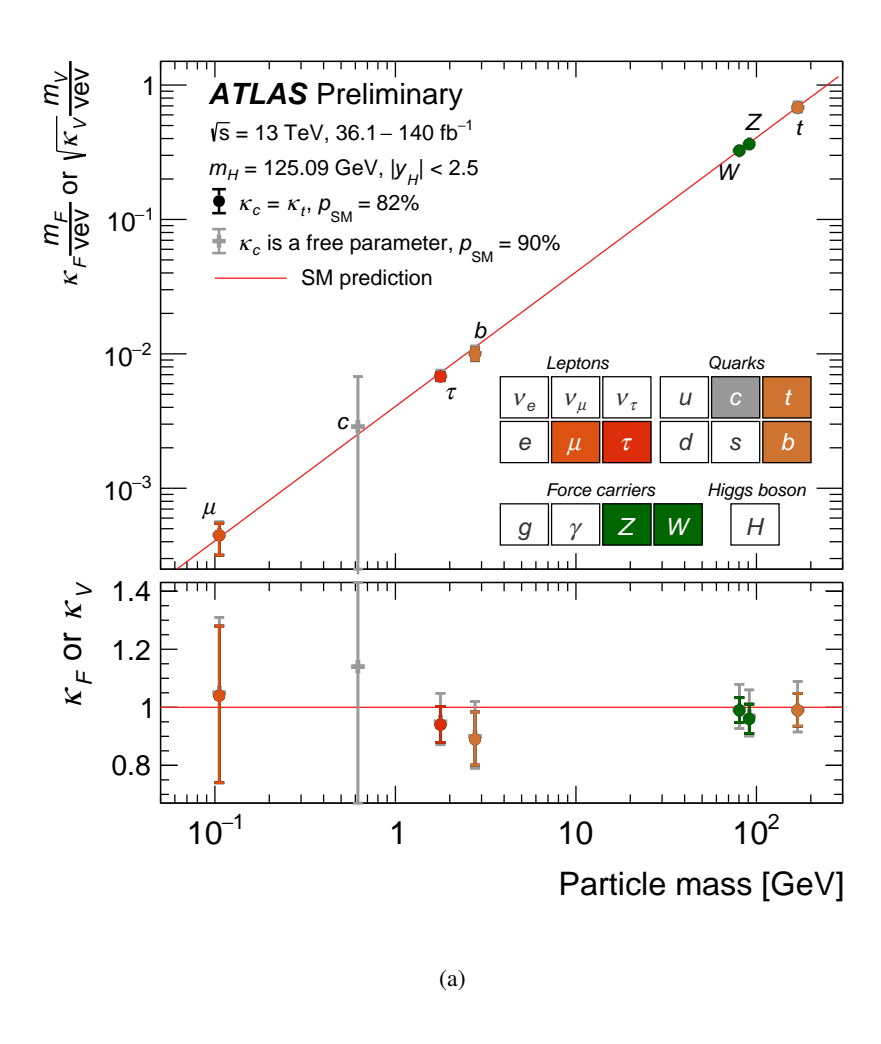


Figure 7: Observed values of Higgs boson coupling modifiers to other SM particles as a function of the particle mass. In the top panel, the values $\kappa_F m_F/v$ and $\sqrt{\kappa_V} m_V/v$ are shown respectively for fermion and boson couplings, where κ_F and κ_V are the coupling modifiers, m_F and m_V are the particle masses, and $v=246\,\text{GeV}$ is the Higgs vacuum expectation value. Quark masses are evaluated in the $\overline{\text{MS}}$ scheme at the scale m_H , while physical masses are used in other cases. The bottom panel shows the raw coupling modifiers. The light gray points show the results in the case where the κ_C modifier is a free parameter in the model, while dark-colored points correspond to the case where κ_C is set equal to κ_I . The resolved parameterization described in the text is used in both cases.

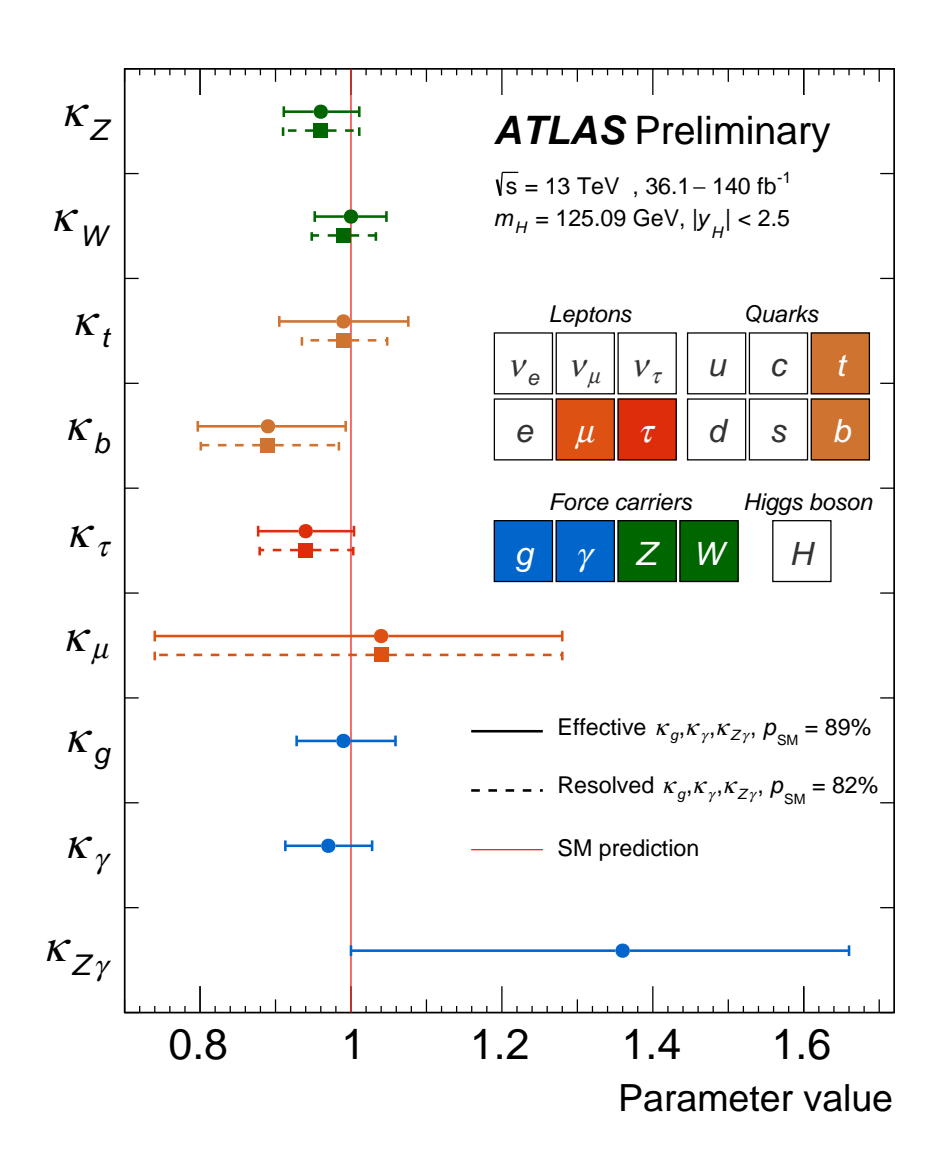


Figure 8: Observed values for Higgs boson coupling modifiers in the resolved parameterization (round markers, solid error bars) and effective parameterization (square markers, dashed error bars). The SM expectation is shown as a vertical red line. Results are shown under the assumption corresponding to the case where κ_c is set equal to κ_t .

Table 5: Observed values of Higgs boson coupling modifiers. The second and third column corresponds to the resolved parameterization, in which the modifiers κ_g , κ_γ and $\kappa_{Z\gamma}$ are expressed as a function of the other modifiers. The fourth column corresponds to the effective parameterization in which the effective modifiers are considered as independent parameters. In the second column, κ_c is included as a measurement parameter, while in the third and fourth columns it is set equal to κ_t .

Parameter	Resolved	$K_g, K_{\gamma}, K_{Z\gamma}$	Effective $\kappa_g, \kappa_{\gamma}, \kappa_{Z\gamma}$	
1 44 44 44 44	Free κ_c	$\kappa_c = \kappa_t$	$\kappa_c = \kappa_t$	
κ_Z	$0.97^{+0.09}_{-0.07}$	0.96 ± 0.05	0.96 ± 0.05	
κ_W	$0.99^{+0.09}_{-0.06}$	0.99 ± 0.04	1.00 ± 0.05	
κ_t	$0.99^{+0.10}_{-0.08}$	$0.99^{+0.06}_{-0.05}$	0.99 ± 0.09	
κ_b	$0.90^{+0.12}_{-0.11}$	0.89 ± 0.09	$0.89^{+0.10}_{-0.09}$	
$\kappa_{ au}$	$0.95^{+0.10}_{-0.08}$	0.94 ± 0.06	0.94 ± 0.06	
κ_c	$1.1^{+1.6}_{-3.8}$		_	
κ_{μ}	$1.05^{+0.25}_{-0.31}$	$1.04^{+0.24}_{-0.30}$	$1.04^{+0.23}_{-0.30}$	
κ_g	_	_	$0.99^{+0.07}_{-0.06}$	
κ_{γ}	_	_	0.97 ± 0.06	
K_{Z/γ^*}	_		$1.36^{+0.30}_{-0.36}$	

5 Conclusion

Higgs boson production and decay rates were measured using up to $140 \, \text{fb}^{-1}$ of pp collision data collected at 13 TeV during Run 2 of the LHC, combining the latest available analyses of each process. The overall Higgs boson signal strength relative to the SM expectation is found to be compatible with SM prediction, and measured with an uncertainty of 6%. The theory uncertainty on the SM prediction of the Higgs boson signal rates is dominant compared to the experimental and statistical contributions.

Cross-sections for Higgs boson production processes are measured to be compatible with the SM, with relative uncertainties ranging between 6% and 18%. Uncertainties on the rates for the WH, ZH, and ttH+tH processes are reduced by about 30%, 20% and 40% respectively, compared to Ref. [3]. Branching fractions into the main Higgs boson decay modes $(H \to \gamma \gamma, H \to ZZ^* \to 4\ell, H \to WW^* \to \ell \nu \ell \nu, H \to bb, H \to \tau \tau)$ were measured with relative uncertainties in the 8%-13% range, and in agreement with SM expectations. The uncertainties in the $H \to bb$ and $H \to WW^*$ branching ratios are reduced by about 20% compared to Ref. [3], and the uncertainty on the $H \to \tau \tau$ branching ratio by 10%. Products of cross-sections and branching ratios for 29 combinations of production and decay channels are also reported.

Interpretations in terms of Higgs boson coupling modifiers are also presented. Assuming only SM contributions to loop processes and Higgs boson processes not probed by the analyses considered here, Higgs boson couplings to W, Z, t, b and τ are measured with uncertainties between 5% and 12%, with improvements ranging from 10% to 20% compared to Ref. [3]. The coupling to the muon is measured with an uncertainty of about 25%. The coupling to the charm quark is measured with an uncertainty of $^{+1.6}_{-3.8}$, corresponding to an improvement by about a factor of 2 compared to Ref. [3]. All results are found to be in agreement with SM predictions.

Appendix

A Coupling modifier parameterization

The parameterization used to express Higgs boson production cross-sections and branching ratios in terms of the coupling modifiers introduced in Section 4.5 is shown in Table 6.

B Expected signal strength results

The expected value of the global signal strength under SM assumptions is

$$\mu = 1.000^{+0.055}_{-0.053} = 1.000 \pm 0.028 \; (\text{stat.}) \; \pm 0.025 \; (\text{exp.}) \; ^{+0.038}_{-0.036} \; (\text{sig. theo.}) \; ^{+0.012}_{-0.013} \; (\text{bkg. theo.}) \; .$$

The corresponding profile log-likelihood scan is shown in Figure 9.

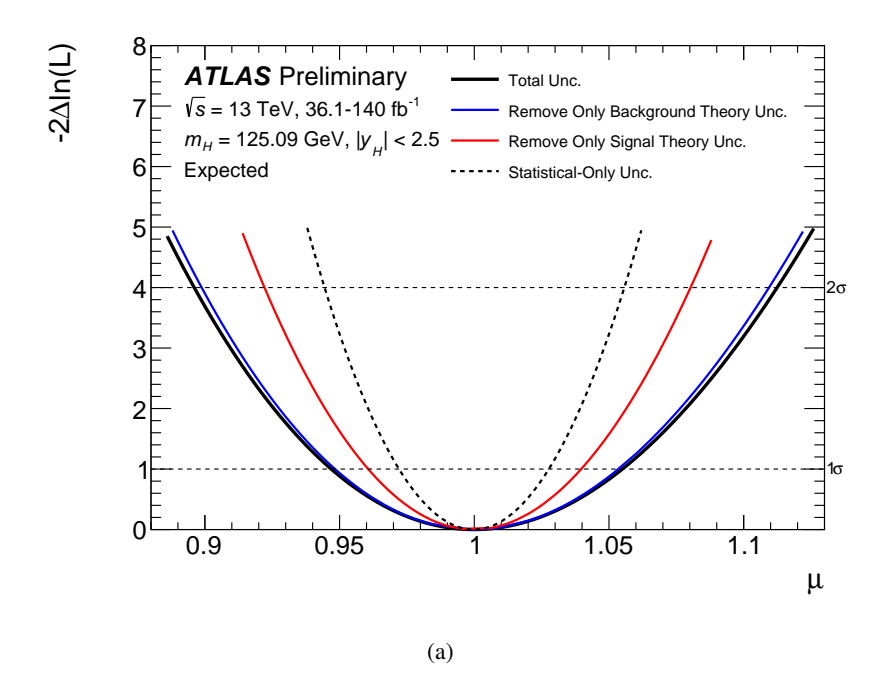


Figure 9: Expected profile log-likelihood value as a function of the signal strength μ , in the model with a single signal-strength scaling all processes. The intersections with the horizontal dotted lines define the 1σ and 2σ uncertainties on the measurement. The solid black line corresponds to the full statistical model with all uncertainties included, and other lines to cases where a class of systematic uncertainties is removed from consideration as described in the text: the background theory uncertainties (blue line), the signal theory uncertainties (red line), and all systematic uncertainties (dashed black line).

Table 6: Parametrizations of Higgs boson production cross sections σ_i at 13 TeV, partial decay widths Γ^f , and the total width Γ_H , normalized to their SM values, as functions of the coupling-strength modifiers κ . The effect of invisible and undetected decays is not considered in the expression for Γ_H . For effective κ parameters associated with loop processes, the resolved scaling in terms of the modifications of the Higgs boson couplings to the fundamental SM particles is given. The coefficients are derived following the methodology in Ref. [40].

Deadystian	Laama	Main	Effective	Resolved modifier	
Production	Loops	interference	modifier	Resolved modifier	
$\sigma(ggF)$	✓	t-b	κ_g^2	$1.040 \kappa_t^2 + 0.002 \kappa_b^2 - 0.038 \kappa_t \kappa_b - 0.005 \kappa_t \kappa_c$	
$\sigma({ m VBF})$	-	-	-	$0.733 \kappa_W^2 + 0.267 \kappa_Z^2$	
$\sigma(qq/qg\to ZH)$	-	-	-	κ_Z^2	
$\sigma(gg \to ZH)$	/	t–Z		$2.456 \kappa_Z^2 + 0.456 \kappa_t^2 - 1.903 \kappa_Z \kappa_t$	
$O\left(gg\to Z\Pi\right)$	V	l-L	-	$-0.011\kappa_Z\kappa_b+0.003\kappa_t\kappa_b$	
$\sigma(WH)$	-	-	-	κ_W^2	
$\sigma(ttH)$	-	-	-	κ_t^2	
$\sigma(tHW)$	-	t– W	-	$2.909 \kappa_t^2 + 2.310 \kappa_W^2 - 4.220 \kappa_t \kappa_W$	
$\sigma(tHq)$	-	t– W	-	$2.633 \kappa_t^2 + 3.578 \kappa_W^2 - 5.211 \kappa_t \kappa_W$	
$\sigma(bbH)$	-	-	-	κ_b^2	
Partial decay width					
Γ^{bb}	-	-	-	κ_b^2	
Γ^{WW}	-	-	-	κ_W^2	
Γ^{gg}	✓	t-b	κ_g^2	$1.111 \kappa_t^2 + 0.012 \kappa_b^2 - 0.1 \kappa_t \kappa_b$	
$\Gamma^{ au au}$	-	-	-	$\kappa_{ au}^2$	
Γ^{ZZ}	-	-	-	κ_Z^2	
Γ^{cc}	-	-	-	κ_c^2	
				$1.589 \kappa_W^2 + 0.072 \kappa_t^2 - 0.674 \kappa_W \kappa_t$	
$\Gamma^{\gamma\gamma}$	✓	t– W	κ_{γ}^2	$+0.009 \kappa_W \kappa_{\tau} + 0.008 \kappa_W \kappa_b$	
				$-0.002\kappa_t\kappa_b-0.002\kappa_t\kappa_\tau$	
$\Gamma^{Z\gamma}$	✓	t– W	$\kappa_{Z\gamma}^2$	$1.118 \kappa_W^2 - 0.125 \kappa_W \kappa_t + 0.004 \kappa_t^2 + 0.003 \kappa_W \kappa_b$	
Γ^{ss}	-	-	-	$\kappa_s^2 (= \kappa_b^2)$	
$\Gamma^{\mu\mu}$	-	-	-	κ_{μ}^2	
Total width					
				$0.581 \kappa_b^2 + 0.215 \kappa_W^2 + 0.082 \kappa_g^2 + 0.063 \kappa_\tau^2$	
Γ_H	✓	-	κ_H^2	$+0.026 \kappa_Z^2 + 0.029 \kappa_c^2 + 0.0023 \kappa_\gamma^2$	
				$+0.0015 \kappa_{(Z\gamma)}^2 + 0.0004 \kappa_s^2 + 0.00022 \kappa_\mu^2$	

C Additional production cross-section and branching ratio results

Expected results under the SM hypothesis for the Higgs boson production cross-sections described in Section 4.2, assuming branching ratios to correspond to SM expectations, are shown in Figure 10. Expected values of the branching ratios described in Section 4.3 assuming the SM value for production cross-sections are shown in Figure 11. Finally, observed and expected results for combinations ($\sigma_i \times B_f$) of production cross-sections σ_i and branching ratios B_f described in Section 4.4 are shown in Figure 12. Observed and expected correlation matrices for the production cross-section results are shown in Figure 13, for branching ratio results in Figure 14 and for products of cross-sections and branching ratios in Figure 15.

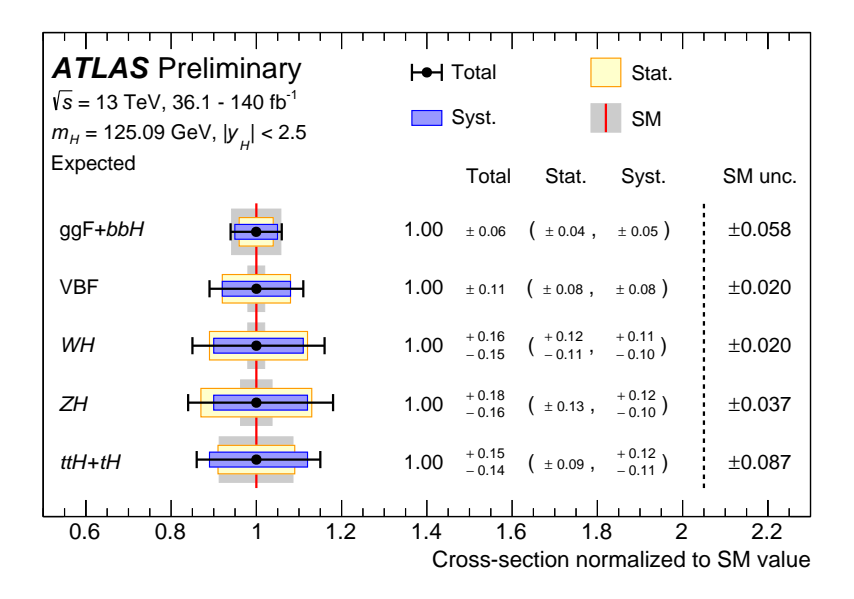


Figure 10: Expected values of the cross-sections for the main Higgs boson production modes, relative to their SM predictions. The bbH mode is considered together with ggF, and tH with ttH. Higgs boson decay branching ratios are assumed to be equal to their SM predictions.

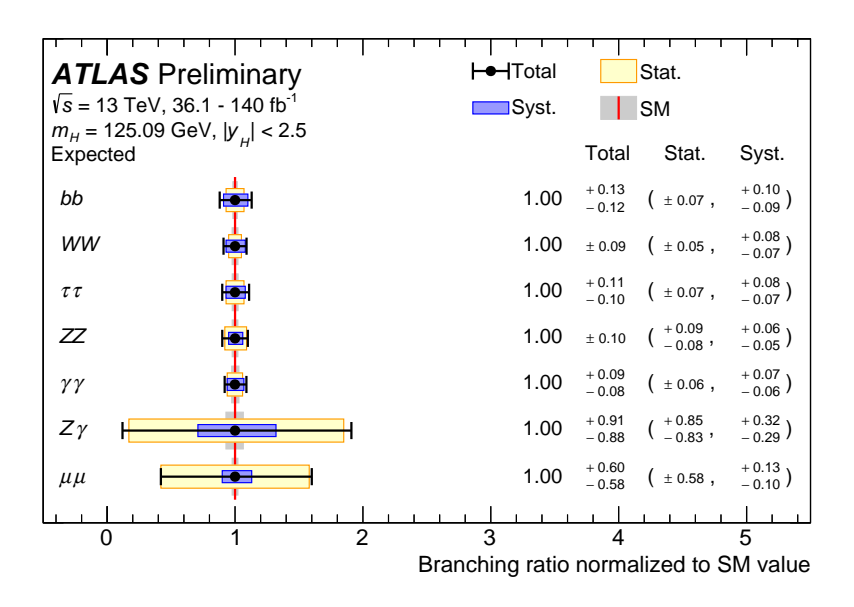


Figure 11: Expected values of the branching ratios in the $H \to bb$, $H \to WW^*$, $H \to \tau\tau$, $H \to ZZ^*$, $H \to \gamma\gamma$, $H \to cc$ and $H \to Z\gamma$ decay modes, relative to their SM predictions. Higgs boson production cross-sections are assumed to be equal to their SM predictions.

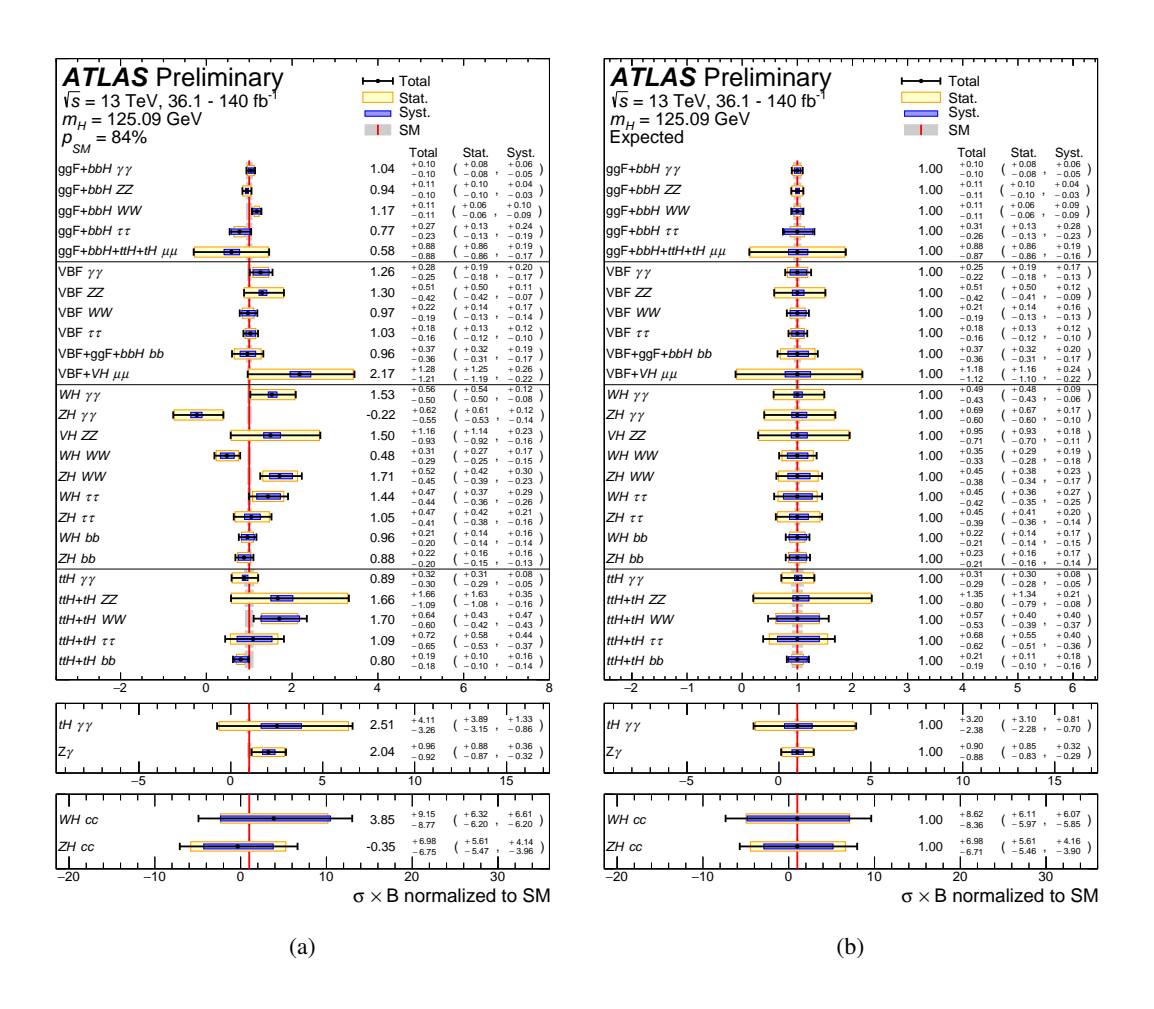


Figure 12: Observed (left) and expected (right) values of the measurements of products of production cross-sections and branching ratios, relative to their SM predictions. The total uncertainties (solid bars) are shown along with their statistical (light shaded regions) and systematic (dark shaded regions) components. Numerical values are shown rounded to two digits after the decimal point.

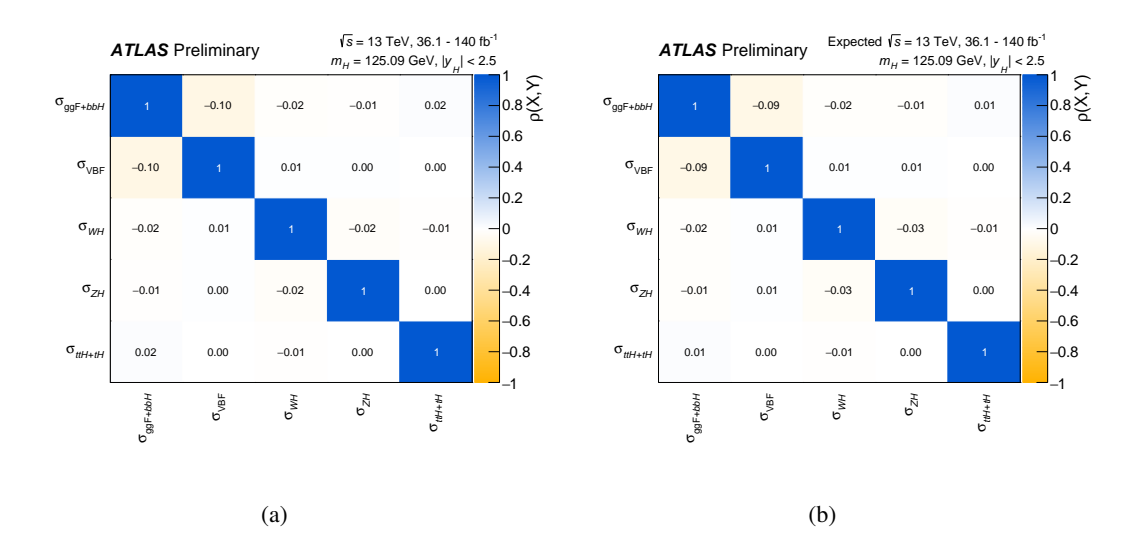


Figure 13: Observed (left) and expected (right) correlation matrices for the measurement of production cross-sections.

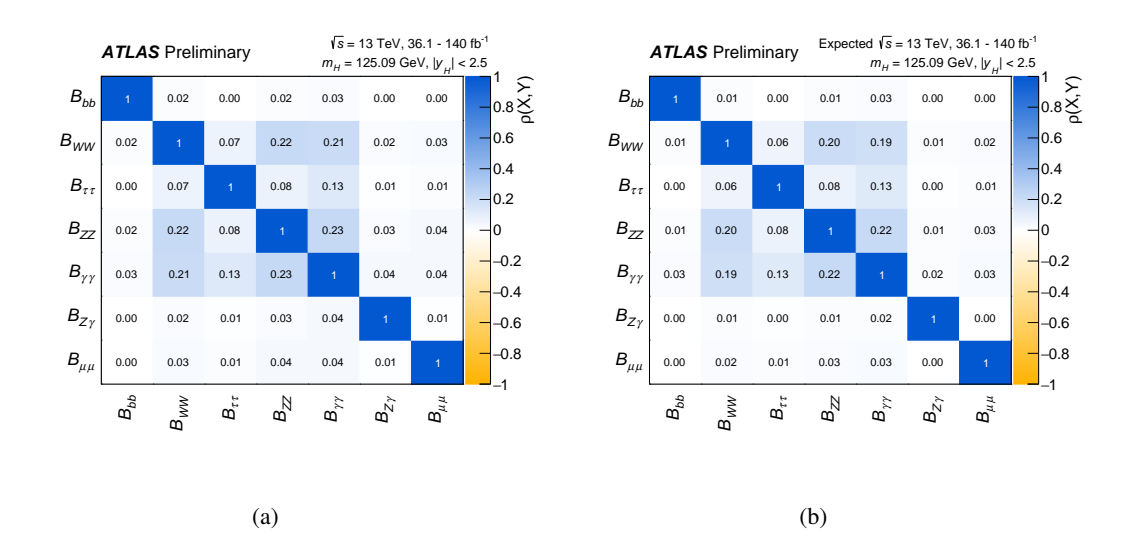


Figure 14: Observed (left) and expected (right) correlation matrices for the measurement of branching ratios.

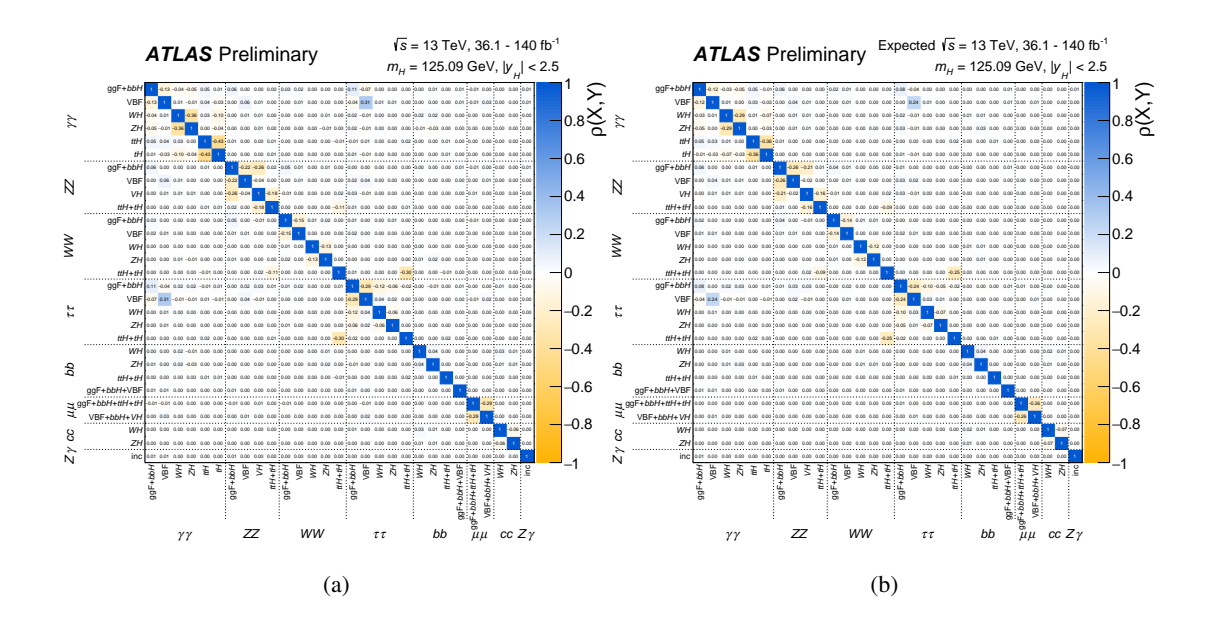


Figure 15: Observed (left) and expected (right) correlation matrices for the measurement of products of products or cross-sections and branching ratios.

D Additional Higgs boson coupling modifier results

For the general coupling modifier models described in Section 4.5, expected results under SM are shown in Table 7. Observed and expected correlation matrices for the resolved model with κ_c included as a measurement parameter, the resolved model with $\kappa_c = \kappa_t$, and the effective model are shown respectively in Figures 16, 17 and 18.

Expected uncertainties on the coupling modifiers in the resolved parameterization are shown in Figure 19 and in the effective parameterization in Figure 20, in both cases together with the corresponding values in Ref. [3].

Table 7: Expected values of Higgs boson coupling modifiers. The second and third column corresponds to the resolved parameterization, in which the modifiers κ_g , κ_γ and $\kappa_{Z\gamma}$ are expressed as a function of the other modifiers. The fourth column corresponds to the effective parameterization in which the effective modifiers are considered as independent parameters. In the second column, κ_c is included as a measurement parameter, while in the third and fourth columns it is set equal to κ_t

Parameter	Resolved	$K_g, K_{\gamma}, K_{Z\gamma}$	Effective $\kappa_g, \kappa_\gamma, \kappa_{Z\gamma}$	
Turumeter	Free κ_c	$\kappa_c = \kappa_t$	$\kappa_c = \kappa_t$	
κ_Z	$1.00^{+0.09}_{-0.07}$	1.00 ± 0.05	1.00 ± 0.05	
κ_W	$1.00^{+0.08}_{-0.06}$	1.00 ± 0.04	1.00 ± 0.05	
κ_t	1.00+0.10	1.00 ± 0.06	1.00+0.08 -0.09	
κ_b	$1.00^{+0.13}_{-0.11}$	1.00 ± 0.10	1.00 ± 0.11	
$\kappa_{ au}$	$1.00^{+0.10}_{-0.08}$	1.00 ± 0.07	1.00 ± 0.07	
K_C	$1.0^{+1.7}_{-3.7}$	-	-	
κ_{μ}	$1.00^{+0.30}_{-0.35}$	$1.00^{+0.26}_{-0.37}$	$1.00^{+0.26}_{-0.37}$	
κ_g	-	-	1.00 ± 0.07	
κ_{γ}	-	-	1.00 ± 0.06	
KZ/γ^*	-	-	$1.0^{+0.4}_{-0.7}$	

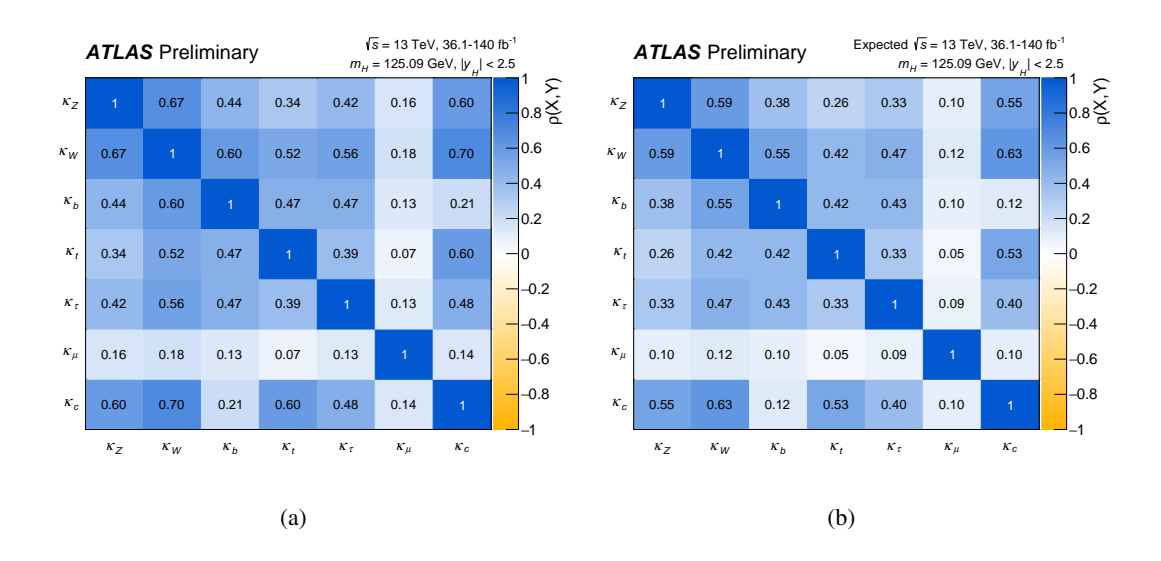


Figure 16: Observed (left) and expected (right) correlation matrices for the measurement of Higgs boson coupling modifiers in the resolved parameterization with κ_c included as a free parameter.

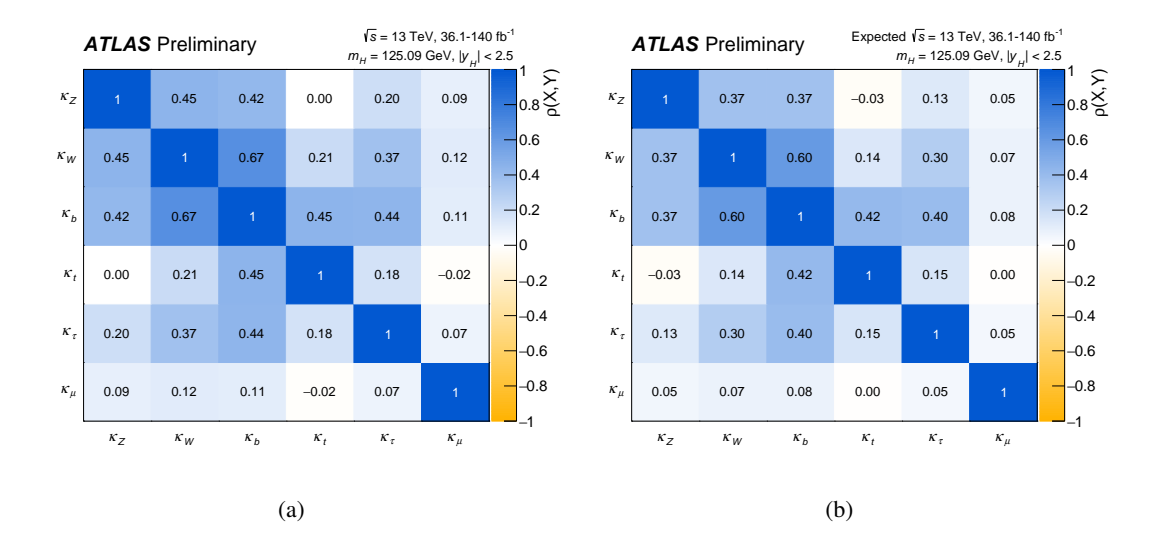


Figure 17: Observed (left) and expected (right) correlation matrices for the measurement of Higgs boson coupling modifiers in the resolved parameterization, assuming $\kappa_c = \kappa_t$.

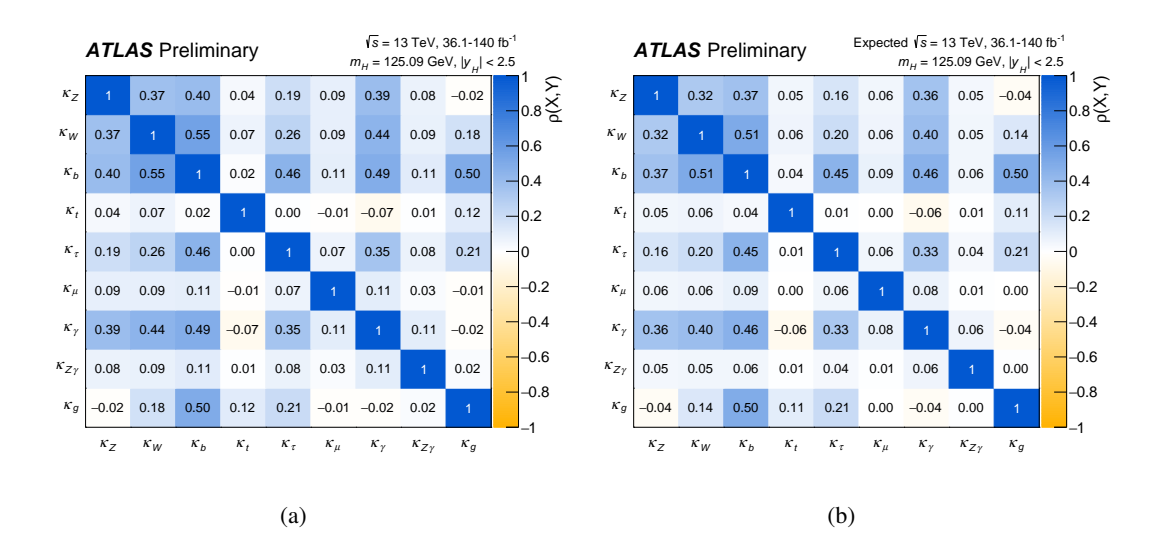


Figure 18: Observed (left) and expected (right) correlation matrices for the measurement of Higgs boson coupling modifiers in the effective parameterization.

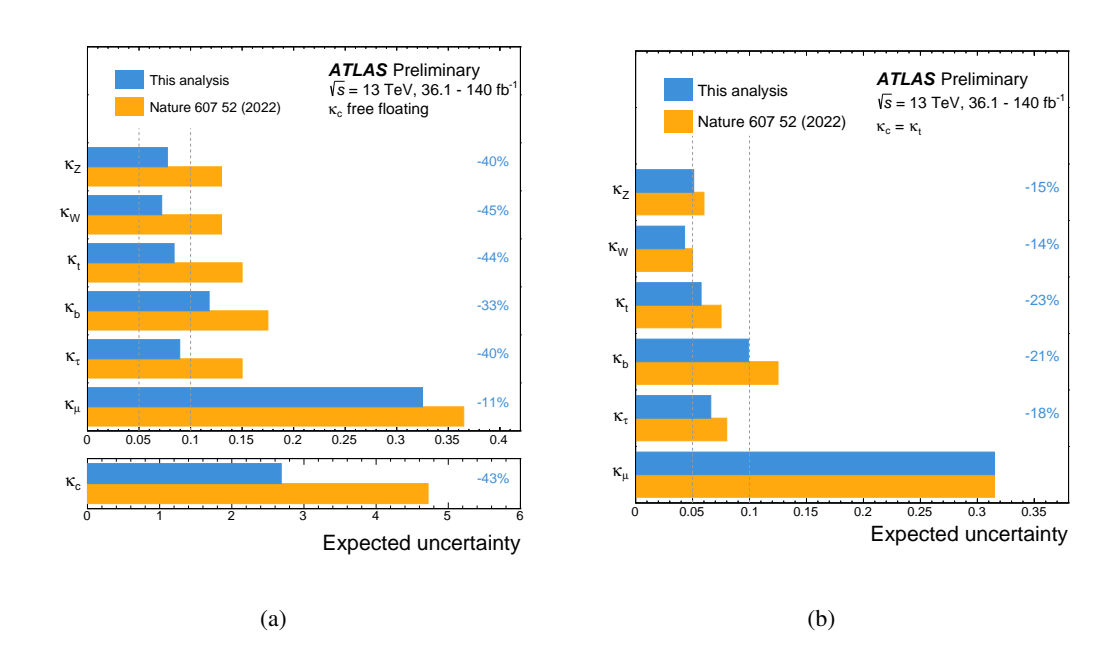


Figure 19: Expected uncertainties on the coupling modifiers in the resolved parameterization including κ_c as a measurement parameter (left) and assuming $\kappa_c = \kappa_t$ (right). Uncertainties are shown for the analysis in this note (top bars, in blue) and for the previous analysis presented in Ref. [3] (bottom bars, in orange). The reduced uncertainty on κ_c in the current analysis is the main driver of the reduction in the uncertainties of the other coupling modifiers, since κ_c indirectly affects their measurement through its effect on the total width of the Higgs boson.

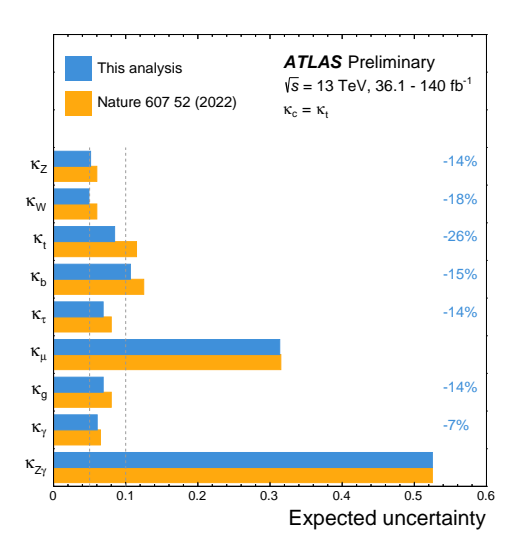


Figure 20: Expected uncertainties on the coupling modifiers in the effective parameterization. Uncertainties are shown for the the analysis in this note (top bars, in blue) and for the previous analysis presented in Ref. [3] (bottom bars, in orange).

E Additional results including partial Run 3 data

This section provides additional plots including the results of two analyses using Run 3 data: an analysis of the $H \to Z\gamma$ channel [41] and an analysis of the $H \to \mu\mu$ channel [42], both performed on a dataset of 165 fb⁻¹ of Run 3 data collected in pp collisions at a center of mass energy $\sqrt{s} = 13.6$ TeV in 2022, 2023 and 2024. In each case, the results are based on a combination of Run 2 and Run 3 results in each channel; the Run 3 results are not included in the overall combination with other channels. The parameterization of the Run 3 analyses in terms of coupling modifiers is performed only on the decay branching ratio, neglecting effects on the production cross-section. Only the relevant coupling modifier ($\kappa_{Z\gamma}$ for the $H \to Z\gamma$ analysis and and κ_{μ} for the $H \to \mu\mu$ analysis) are free to vary in the fit. The Higgs boson total width is defined by setting $\kappa_b = 0.89$, the best-fit value in the combination of Run 2 analyses, and other modifiers to unity. The effect of these assumptions is expected to be negligible compared to the reported uncertainties on the coupling modifiers. The SM predictions for the production cross-sections at $\sqrt{s} = 13.6$ TeV are computed using the same methodology as for the Run 2 results.

Figure 21 shows measurements of Higgs boson branching ratios, Figure 22 Higgs boson coupling modifiers in the resolved parameterization as a function of particle mass, Figure 23 the measured values of coupling modifiers in the effective parameterization, and Figure 24 their expected uncertainties.

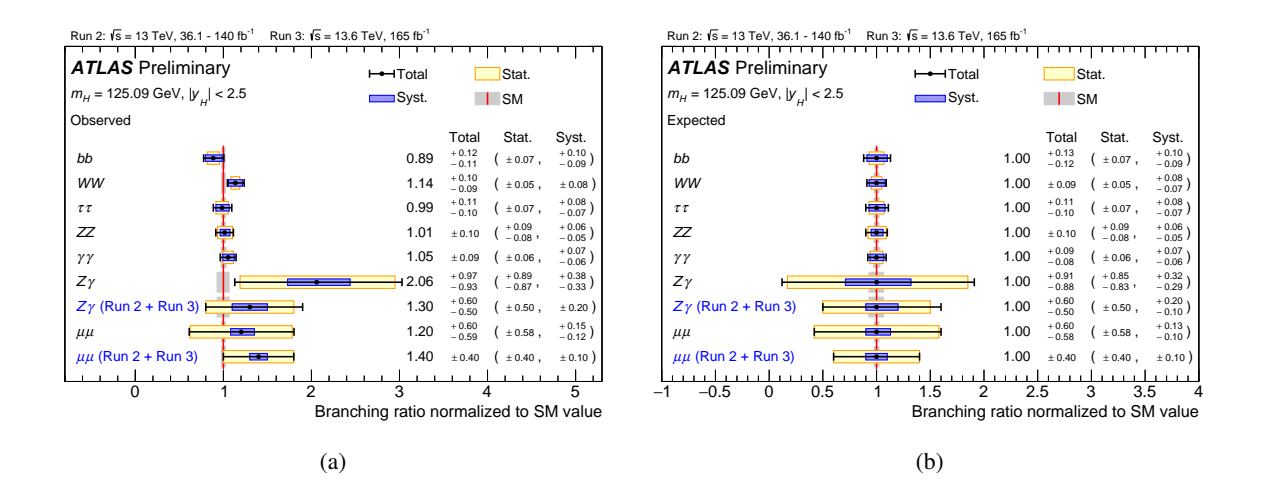


Figure 21: Observed (left) and expected (right) values of the branching ratios in the $H \to bb$, $H \to WW^*$, $H \to \tau\tau$, $H \to ZZ^*$, $H \to \gamma\gamma$, $H \to Z\gamma$ and $H \to \mu\mu$ decay modes, relative to their SM predictions. Higgs boson production cross-sections are assumed to be equal to their SM predictions. For $H \to Z\gamma$ and $H \to \mu\mu$, results including Run 3 data are also shown. The parameterization of the Run 3 analyses in terms of coupling modifiers is performed only on the decay branching ratio, neglecting effects on the production cross-section. Only the relevant coupling modifier ($\kappa_{Z\gamma}$ for the $H \to Z\gamma$ analysis and and κ_{μ} for the $H \to \mu\mu$ analysis) are free to vary in the fit. The Higgs boson total width is defined by setting $\kappa_b = 0.89$, the best-fit value in the combination of Run 2 analyses, and other modifiers to unity.

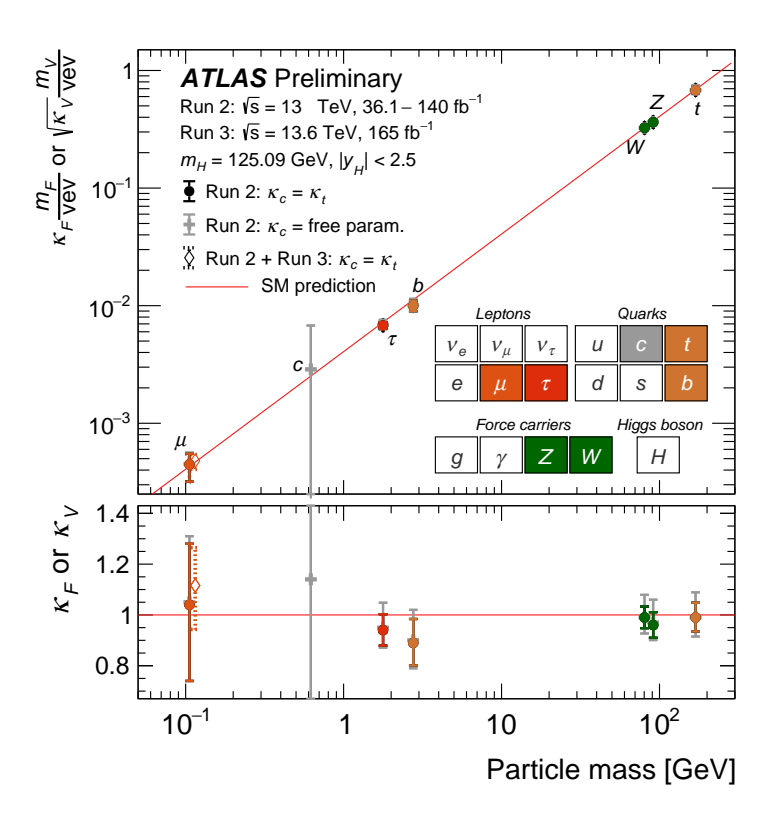


Figure 22: Observed values of Higgs boson coupling modifiers to other SM particles as a function of the particle mass. In the top panel, the values $\kappa_F m_F/v$ and $\sqrt{\kappa_V} m_V/v$ are shown respectively for fermion and boson couplings, where κ_F and κ_V are the coupling modifiers, m_F and m_V are the particle masses, and $v=246\,\mathrm{GeV}$ is the Higgs vacuum expectation value. Quark masses are evaluated in the $\overline{\mathrm{MS}}$ scheme at the scale m_H , while physical masses are used in other cases. The bottom panel shows the raw coupling modifiers. The grey points and error bars show the results in the case where the κ_C modifier is a free parameter in the model, while dark-colored markers correspond to the case where κ_C is set equal to κ_t . The resolved parameterization described in the text is used in both cases. A measurement of κ_μ including Run 3 data also included as mentioned in the text is shown with an empty marker and dotted error bars.

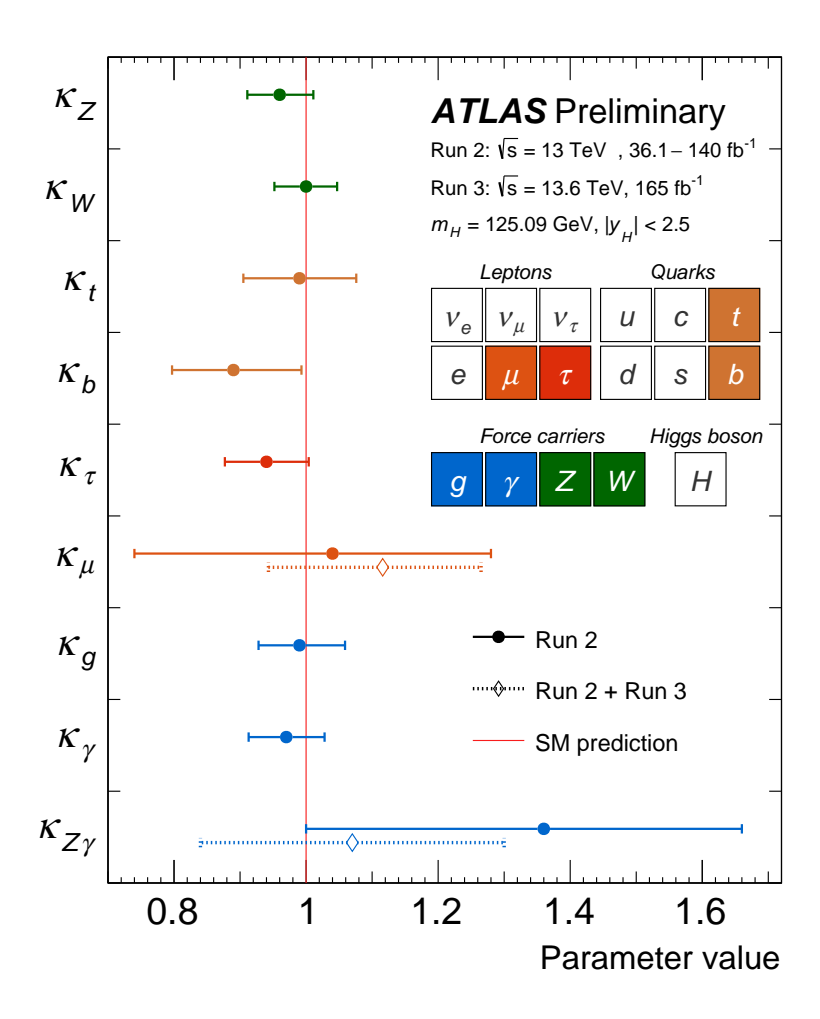


Figure 23: Measured values of coupling modifiers in the effective parameterization. For $\kappa_{Z\gamma}$ and κ_{μ} , results including Run 3 data as mentioned in the text are also shown in dashed lines. Results are shown under the assumption corresponding to the case where κ_c is set equal to κ_t .

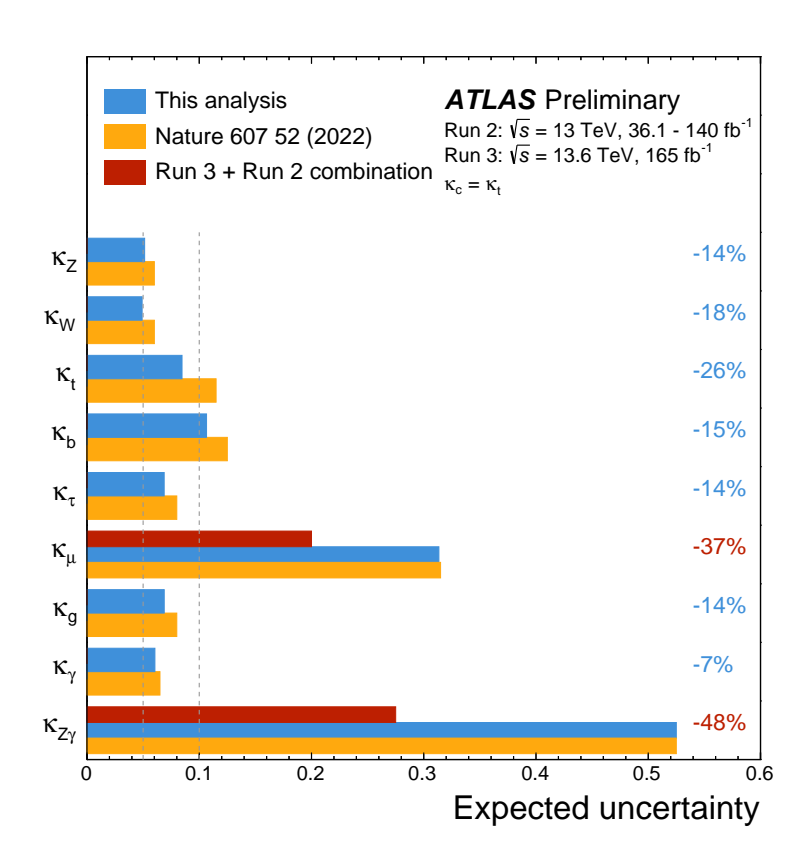


Figure 24: Expected uncertainties on the coupling modifiers in the effective parameterization for the analysis in this note (blue bars) and for the previous analysis presented in Ref. [3] (orange bars). For $\kappa_{Z\gamma}$ and κ_{μ} , results including Run 3 data as mentioned in the text are also shown (red bars).

References

- [1] ATLAS Collaboration, Observation of a new particle in the search for the Standard Model Higgs boson with the ATLAS detector at the LHC, Phys. Lett. B **716** (2012) 1, arXiv: 1207.7214 [hep-ex] (cit. on p. 2).
- [2] CMS Collaboration,

 Observation of a new boson at a mass of 125 GeV with the CMS experiment at the LHC,

 Phys. Lett. B 716 (2012) 30, arXiv: 1207.7235 [hep-ex] (cit. on p. 2).
- [3] ATLAS Collaboration,

 A detailed map of Higgs boson interactions by the ATLAS experiment ten years after the discovery,

 Nature 607 (2022) 52, arXiv: 2207.00092 [hep-ex] (cit. on pp. 3, 5–8, 12, 17, 25, 27, 28, 32),

 Erratum: Nature 612 (2022) E24.
- [4] ATLAS Collaboration, Evidence for the associated production of the Higgs boson and a top quark pair with the ATLAS detector, Phys. Rev. D **97** (2018) 072003, arXiv: 1712.08891 [hep-ex] (cit. on pp. 3, 5).
- [5] ATLAS Collaboration, *Measurements of Higgs bosons decaying to bottom quarks from vector boson fusion production with the ATLAS experiment at* $\sqrt{s} = 13$ TeV, Eur. Phys. J. C **81** (2021) 537, arXiv: 2011.08280 [hep-ex] (cit. on pp. 3, 5).
- [6] ATLAS and CMS Collaborations, Combined Measurement of the Higgs Boson Mass in pp Collisions at $\sqrt{s} = 7$ and 8 TeV with the ATLAS and CMS Experiments, Phys. Rev. Lett. **114** (2015) 191803, arXiv: 1503.07589 [hep-ex] (cit. on p. 3).
- [7] ATLAS Collaboration, Combined Measurement of the Higgs Boson Mass from the $H \to \gamma \gamma$ and $H \to ZZ^* \to 4\ell$ Decay Channels with the ATLAS Detector Using $\sqrt{s} = 7, 8$, and 13 TeV pp Collision Data, Phys. Rev. Lett. **131** (2023) 251802, arXiv: 2308.04775 [hep-ex] (cit. on p. 3).
- [8] ATLAS Collaboration, Measurement of the Higgs boson mass in the $H \to ZZ^* \to 4\ell$ decay channel using $139 \, fb^{-1}$ of $\sqrt{s} = 13 \, \text{TeV}$ pp collisions recorded by the ATLAS detector at the LHC, Phys. Lett. B **843** (2023) 137880, arXiv: 2207.00320 [hep-ex] (cit. on p. 3).
- [9] CMS Collaboration, A measurement of the Higgs boson mass in the diphoton decay channel, Phys. Lett. B **805** (2020) 135425, arXiv: 2002.06398 [hep-ex] (cit. on p. 3).
- [10] CMS Collaboration, Measurement of the Higgs boson mass and width using the four-lepton final state in proton–proton collisions at $\sqrt{s} = 13$ TeV, (2024), arXiv: 2409.13663 [hep-ex] (cit. on p. 3).
- [11] LHC Higgs Cross Section Working Group, S. Heinemeyer et al., Handbook of LHC Higgs Cross Sections: 3. Higgs Properties, CERN-2013-004 (2013), arXiv: 1307.1347 [hep-ph] (cit. on p. 3).
- [12] ATLAS Collaboration, *The ATLAS Experiment at the CERN Large Hadron Collider*, JINST **3** (2008) S08003 (cit. on p. 3).
- [13] ATLAS Collaboration, *Operation of the ATLAS trigger system in Run* 2, JINST **15** (2020) P10004, arXiv: 2007.12539 [physics.ins-det] (cit. on p. 4).
- [14] ATLAS Collaboration, *The ATLAS Collaboration Software and Firmware*, ATL-SOFT-PUB-2021-001, 2021, url: https://cds.cern.ch/record/2767187 (cit. on p. 4).

- [15] J. R. Andersen et al., Les Houches 2015: Physics at TeV Colliders Standard Model Working Group Report, (2016), arXiv: 1605.04692 [hep-ph] (cit. on p. 4).
- [16] LHC Higgs Cross Section Working Group, D. de Florian et al., Handbook of LHC Higgs Cross Sections: 4. Deciphering the Nature of the Higgs Sector, (2016), arXiv: 1610.07922 [hep-ph] (cit. on pp. 4, 6).
- [17] N. Berger et al., Simplified Template Cross Sections Stage 1.1, (2019), arXiv: 1906.02754 [hep-ph] (cit. on p. 4).
- [18] ATLAS Collaboration,

 Luminosity determination in pp collisions at $\sqrt{s} = 13$ TeV using the ATLAS detector at the LHC,

 Eur. Phys. J. C 83 (2023) 982, arXiv: 2212.09379 [hep-ex] (cit. on p. 4).
- [19] ATLAS Collaboration, Higgs boson production cross-section measurements and their EFT interpretation in the 4 ℓ decay channel at $\sqrt{s} = 13$ TeV with the ATLAS detector, Eur. Phys. J. C **80** (2020) 957, arXiv: 2004.03447 [hep-ex] (cit. on p. 5), Erratum: Eur. Phys. J. C **81** (2021) 29, Erratum: Eur. Phys. J. C **81** (2021) 398.
- [20] ATLAS Collaboration, Measurements of Higgs boson production via gluon-gluon fusion and vector-boson fusion using $H ound WW^* ound \ell \nu\ell\nu$ decays in pp collisions with the ATLAS detector and their effective field theory interpretations, (2025), arXiv: 2504.07686 [hep-ex], URL: https://cds.cern.ch/record/2919068 (cit. on pp. 5, 8).
- [21] ATLAS Collaboration, Measurements of the production cross-sections of a Higgs boson in association with a vector boson and decaying into WW* with the ATLAS detector at $\sqrt{s} = 13$ TeV, (2025), arXiv: 2503.19420 [hep-ex] (cit. on pp. 5, 9).
- [22] ATLAS Collaboration, Measurement of the properties of Higgs boson production at $\sqrt{s} = 13$ TeV in the $H \rightarrow \gamma \gamma$ channel using 139 fb⁻¹ of pp collision data with the ATLAS experiment, JHEP **07** (2023) 088, arXiv: 2207.00348 [hep-ex] (cit. on p. 5).
- [23] ATLAS Collaboration, A search for the Zy decay mode of the Higgs boson in pp collisions at $\sqrt{s} = 13$ TeV with the ATLAS detector, Phys. Lett. B **809** (2020) 135754, arXiv: 2005.05382 [hep-ex] (cit. on p. 5).
- [24] ATLAS Collaboration, Differential cross-section measurements of Higgs boson production in the $H \to \tau^+ \tau^-$ decay channel in pp collisions at $\sqrt{s} = 13$ TeV with the ATLAS detector, JHEP **03** (2025) 010, arXiv: 2407.16320 [hep-ex] (cit. on pp. 5, 8).
- [25] ATLAS Collaboration,

 Measurement of the VH, $H \rightarrow \tau\tau$ process with the ATLAS detector at 13 TeV,

 Phys. Lett. B **855** (2024) 138817, arXiv: 2312.02394 [hep-ex] (cit. on pp. 5, 9).
- [26] ATLAS Collaboration,

 A search for the dimuon decay of the Standard Model Higgs boson with the ATLAS detector,
 Phys. Lett. B 812 (2021) 135980, arXiv: 2007.07830 [hep-ex] (cit. on p. 5).
- [27] ATLAS Collaboration,

 Measurements of WH and ZH production with Higgs boson decays into bottom quarks and direct constraints on the charm Yukawa coupling in 13 TeV pp collisions with the ATLAS detector,

 JHEP 04 (2025) 075, arXiv: 2410.19611 [hep-ex] (cit. on pp. 5, 7, 8, 12).

- [28] ATLAS Collaboration,

 Measurement of the associated production of a top-antitop-quark pair and a Higgs boson decaying into a $b\bar{b}$ pair in pp collisions at $\sqrt{s} = 13$ TeV using the ATLAS detector at the LHC,

 Eur. Phys. J. C 85 (2025) 210, arXiv: 2407.10904 [hep-ex] (cit. on pp. 5, 7, 8).
- [29] K. Kudashkin, J. M. Lindert, K. Melnikov and C. Wever, Higgs bosons with large transverse momentum at the LHC, Phys. Lett. B **782** (2018) 210, arXiv: 1801.08226 [hep-ph] (cit. on p. 4).
- [30] A. Djouadi, J. Kalinowski, M. Mühlleitner and M. Spira, *HDECAY: Twenty++ years after*, Comput. Phys. Commun. **238** (2019) 214, arXiv: 1801.09506 [hep-ph] (cit. on p. 4).
- [31] M. Bonetti, K. Melnikov and L. Tancredi, *Higher order corrections to mixed QCD-EW contributions to Higgs boson production in gluon fusion*, Phys. Rev. D **97** (2018) 056017, arXiv: 1801.10403 [hep-ph] (cit. on p. 4), Erratum: Phys. Rev. D **97** (2018) 099906(E).
- [32] F. Dulat, A. Lazopoulos and B. Mistlberger, *iHixs 2 Inclusive Higgs cross sections*, Comput. Phys. Commun. **233** (2018) 243, arXiv: 1802.00827 [hep-ph] (cit. on p. 4).
- [33] R. V. Harlander, J. Klappert, S. Liebler and L. Simon, *vh@nnlo-v2: new physics in Higgs Strahlung*, JHEP **05** (2018) 089, arXiv: 1802.04817 [hep-ph] (cit. on p. 4).
- [34] M. Cacciari, F. A. Dreyer, A. Karlberg, G. P. Salam and G. Zanderighi, Fully differential Vector-Boson-Fusion Higgs production at Next-to-Next-to-Leading Order, Phys. Rev. Lett. 115 (2015) 082002, arXiv: 1506.02660 [hep-ph], Erratum: Phys. Rev. Lett. 120 (2018) 139901 (cit. on p. 4).
- [35] ATLAS and CMS Collaborations,

 Procedure for the LHC Higgs boson search combination in Summer 2011, tech. rep., 2011,

 URL: http://cdsweb.cern.ch/record/1375842 (cit. on p. 5).
- [36] G. Cowan, K. Cranmer, E. Gross and O. Vitells, *Asymptotic formulae for likelihood-based tests of new physics*, Eur. Phys. J. C **71** (2011) 1554, arXiv: 1007.1727 [physics.data-an], Erratum: Eur. Phys. J. C73 (2013) 2501 (cit. on p. 5).
- [37] ATLAS and CMS Collaborations, Measurements of the Higgs boson production and decay rates and constraints on its couplings from a combined ATLAS and CMS analysis of the LHC pp collision data at $\sqrt{s} = 7$ and 8 TeV, JHEP **08** (2016) 045, arXiv: 1606.02266 [hep-ex] (cit. on p. 12).
- [38] ATLAS Collaboration, Determination of the Relative Sign of the Higgs Boson Couplings to W and Z Bosons Using WH Production via Vector-Boson Fusion with the ATLAS Detector, Phys. Rev. Lett. 133 (2024) 141801, arXiv: 2402.00426 [hep-ex] (cit. on p. 12).
- [39] CMS Collaboration, Study of WH production through vector boson scattering and extraction of the relative sign of the W and Z couplings to the Higgs boson in proton–proton collisions at $\sqrt{s} = 13$ TeV, Phys. Lett. B **860** (2025) 139202, arXiv: 2405.16566 [hep-ex] (cit. on p. 12).
- [40] J. R. Andersen et al., *Handbook of LHC Higgs Cross Sections: 3. Higgs Properties*, (2013), ed. by S. Heinemeyer, C. Mariotti, G. Passarino and R. Tanaka, arXiv: 1307.1347 [hep-ph] (cit. on p. 19).
- [41] ATLAS Collaboration, Search for the Higgs boson decay to a Z boson and a photon in pp collisions at $\sqrt{s} = 13$ TeV and 13.6 TeV with the ATLAS detector, ATLAS-CONF-2025-007, 2025 (cit. on p. 29).

[42] ATLAS Collaboration,

Evidence for the dimuon decay of the Higgs boson in pp collisions with the ATLAS detector, CERN-EP-2025-149, 2025 (cit. on p. 29).